AD-A136 123 MULTIPOLE MONOLITHIC SURFACE ACOUSTIC WAVE (SAW) RESONATOR FILTERS(U) SPERRY RESEARCH CENTER SUDBURY MA P C MEYER ET AL. OCT 83 SRC-CR-83-39 N00014-81-C-2066 1/1

UNCLASSIFIED F/G 9/5 NL

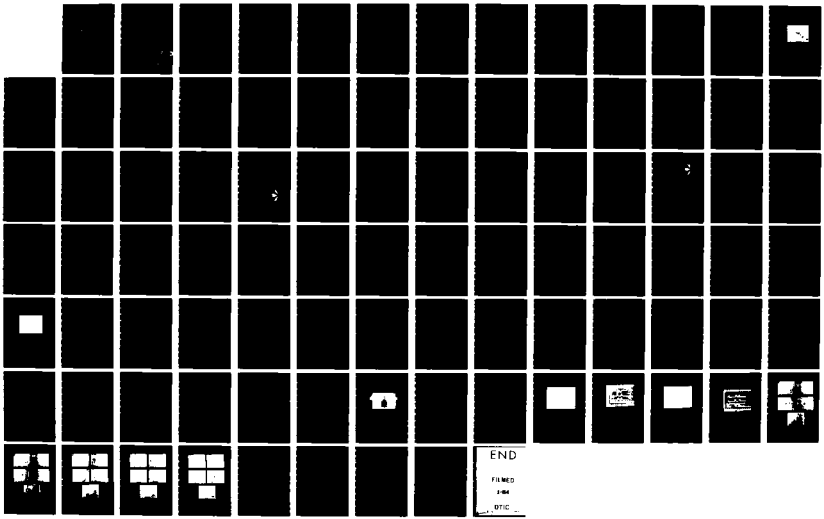

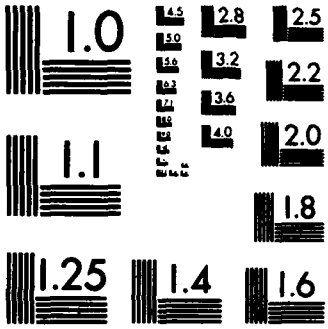

MICROCOPY RESOLUTION TEST CHART
NATIONAL BUREAU OF STANDARDS-1963-A

AD-A136123

12

MULTIPOLE MONOLITHIC SURFACE ACOUSTIC WAVE (SAW) RESONATOR FILTERS

P. C. Meyer, W. J. Tanski and D. Gunes
Sperry Research Center, Sudbury, MA 01776

Final Report
Contract No. N00014-81-C-2066

SRC-CR-83-39
October 1983

Prepared for
Naval Research Laboratory
Washington, DC 20375

DTIC
ELECTE
DEC 21 1983
S D
D

SPERRY
RESEARCH CENTER

DTIC FILE COPY

DISTRIBUTION STATEMENT A
Approved for public release;
Distribution Unlimited

83 11 21 013

TABLE OF CONTENTS

Section		Page
1	INTRODUCTION	1
2	SAW MULTIPOLE FILTER DESIGN	3
	2.1 Filter Synthesis Techniques	3
	2.2 Type I Filter Design	4
	2.3 Analysis	19
3	MULTIPOLE RESONATOR FILTER MODELING	36
	3.1 Lumped Element Model	36
	3.2 Type I Filter Model Results	48
4	DEVICE FABRICATION	58
	4.1 Photolithography	58
	4.2 Frequency Trimming	63
	4.3 Packaging of Phase I Devices	66
	4.4 Packaging of Phase II Devices	69
5	EXPERIMENTAL TEST RESULTS	71
	5.1 Test Results of the Delivered Type I Filters	71
6	CONCLUSION	82
	REFERENCES	84

Accession For
NTIS GRA&I ☒
DTIC TAB ☐
Unannounced ☐
Justification
By Per Ltr. on File
Distribution/
Availability Codes
Dist | Avail and/or Special
A/1

DTIC COPY INSPECTED 3

LIST OF ILLUSTRATIONS

Figure		Page
1	Schematic showing the four-pole configuration with two transducer-coupled cavity-pairs and one pair coupled by a reflector.	1
2	Schematic showing the six-pole configuration with two transducer-coupled cavity-pairs and three pair, coupled acoustically.	6
3	Out-of-band rejection of one two-pole section with cosine weighting of reflector ends and cosine weighted transducers.	7
4	Schematic diagram required to understand the matching circuit.	16
5	Schematic representation of our scheme for efficient computation of the response of a multipole filter.	21
6	Computed narrowband response for Type II with component values given on Fig. 1.	23
7	Computed response for Type II with component values as given on Fig. 1.	23
8	Computed wideband response for Type II with component values as given in Fig. 1.	24
9	Voltage standing wave ratio (VSWR) for Type II.	26
10	Smith chart plot of the input (and output) impedances for Type II as shown on Fig. 1.	26
11	Computed response of the acoustically-coupled cavity-pair for Type II (central portion of Fig. 1) unmatched.	27
12	Computed reflection coefficient magnitude, / /, for cavity No. 2 of Type II (central section of Fig. 1) of the acoustically-coupled pair with cavity No. 3 electrically unloaded.	27
13	Computed response for one of the two-port resonators of Type II (Fig. 1) unmatched into 50 ohms.	28
14	Computed narrowband response for Type I with component values given on Fig. 2.	31
15	Computed response for Type I with component values as shown on Fig. 1.	31
16	Computed wideband response for Type I with component values as on Fig. 2.	32
17	Voltage stand wave ratio (VSWR) for Type I.	32

LIST OF ILLUSTRATIONS (Continued)

Figure		Page
18	Smith chart of the input (and output) impedances for Type I, as shown on Fig. 2.	33
19	Computed response of the acoustically-coupled cavities No. 1 and 2 (or 5 and 6) for Type I, electrically unmatched into 50 ohms.	33
20	Computed reflection coefficient magnitude, / /, for cavity No. 1 of Type I (the input in the upper left of Fig. 2) with cavity No. 2 electrically unloaded.	34
21	Computed reflection coefficient magnitude, / /, for cavity No. 2 of Type I with cavity No. 1 electrically unloaded.	34
22	Computed response of the acoustically-coupled cavity-pair (No. 3 and 4 of Fig. 2) for Type I, electrically unmatched.	35
23	Computed reflection coefficient magnitude, / /, for Type I cavity No. 3 of Fig. 2 with cavity No. 4 electrically unloaded.	35
24	Equivalent circuit model of an acoustically coupled two-pole section.	37
25	Theoretical broadband attenuation characteristics of the six-pole filter (matched into 50 ohms) with resonator Q = ≅ 18,000 (in atmosphere).	42
26	Six-pole filter constructed of two-pole sections.	44
27	Six-pole filter with input/output matching and 50-ohm terminations.	46
28	Theoretical six-pole filter input reflection coefficient magnitude plot with both input and output loaded by 50 ohms and with no matching.	46
29	Theoretical passband response of the six-pole filter loaded at the input and the output by 50 ohms without any matching.	49
30	Theoretical passband transmission characteristics of the six-pole (matched into 50 ohms) with resonator Q ≅ 18,000 (in atmosphere).	49
31	Measured amplitude and return loss for unmatched six-pole filter.	50
32	Passband transmission response for middle section of filter.	52
33	Input return loss (20 log s_{11}) for middle section of filter.	53

LIST OF ILLUSTRATIONS (Continued)

Figure		Page
34	Passband transmission response for input/output section of filter.	54
35	Input return loss (20 log s_{11}) for first cavity of input/output section.	55
36	Input return loss (20 s_{11}) for second cavity of input/output section.	56
37	Process steps required for fabrication of a recessed-transducer/grooved-reflector resonator system.	60
38	Section view illustrating a technique for varying the coupling (by changing the groove depth) of grooved grating-couplers on quartz.	62
39	Section view of the resonator configuration before and after selectively etching the quartz substrate in a tetrafluormethane (CF_4)-plus-oxygen plasma.	62
40	Deeply recessed transducer (a) before RIE trimming and (b) after RIE trimming.	65
41	Resonant frequency vs. substrate distance (h) from top of metal film for a single pole, two-pole test resonator.	65
42	Diagram of the cold-weld-sealable Type D leader.	68
43	Device No. 2 packaged in flatpack and brass block. Input and output matching components are outside the flatpack.	70
44	Device 1 mounted in flatpack.	73
45	Device 2 mounted in flatpack.	74
46	Device 3 mounted in flatpack.	75
47	Device 4 mounted in flatpack.	76
48	Measured response of filter No. 1.	77
49	Measured response of filter No. 2.	78
50	Measured response of filter No. 3.	79
51	Measured response of filter No. 4.	80
52	Measured response of filter No. 5.	81

SECTION 1

INTRODUCTION

This final report describes the work done and results achieved on a two-year effort to design and fabricate monolithic multipole Surface Acoustic Wave (SAW) resonator filters. The work and the report focus on two specific filter designs: one a six-pole Butterworth design at a center frequency of 217 MHz (Type I), the other a four-pole Chebyshev at 150 MHz (Type II). The specifications are listed ~~in Table I~~. However, the design, testing, and fabrication techniques used are general and would apply equally well to similar SAW resonator filters in the 100 MHz to 800 MHz frequency range. Since more work was done, and the best results achieved on the 217 MHz Butterworth filter, it will be treated in more detail.

Multipole SAW resonator technology can be divided logically into three technical areas, each with its own body of existing knowledge: (1) multipole filter synthesis, (2) SAW resonator analysis and design, and (3) fabrication and packaging techniques. Where feasible, the experience and techniques already developed in other technologies have been adapted for SAW multipole design and fabrication. In particular there are many similarities between bulk wave multipole filters and the SAW counterparts. In both technologies good process control and computer modeling are essential elements in providing the accuracy and precision required to achieve a multipole design. While a monolithic approach to multipole filter fabrication would be desireable, the state-of-the-art in resonator fabrication is not exact enough to provide acceptable results, hence a two-pole building block approach has been used, which for bulk wave resonator filters has been called a polylithic approach[9].

Table I

Filter Specifications

	Type I	Type II
Passband Center Frequency (F_r)	217 MHz	150 MHz
3 dB Bandwidth (ΔF_3)	40 kHz (Q_f = 5400)	37 kHz (Q_f = 4050)
Shape Factor (60dB / 3dB)	4/1	8.1/1
Maximum Insertion Loss	10 dB	6 dB
Filter Response	Butterworth	Chebyshev (1.5dB ripple)
Minimum Rejection beyond		
$F_R \pm 0.15$ MHz		60 dB
$F_R \pm 0.5$ MHz		80 dB
$F_R \pm 5.0$ MHz		110 dB
Package Size		Minimum Possible
Input/Output Impedance	50 ohms	50 ohms
Operational Temperature Range	10 to 40°C	-10 to 80°C
Filter-to-Filter Phase Difference	10° (over 3 dB bandwidth)	

SECTION 2
SAW MULTIPOLE FILTER DESIGN

2.1 FILTER SYNTHESIS TECHNIQUES

Generalized filter synthesis is a mature technology and a detailed examination of it is outside the scope of this study. Characteristics of common filter types, such as Bessel, Gaussian, Chebyshev, and Butterworth filters are tabulated in several handbooks[1,2,3]. The desired filter characteristics are matched to the appropriate filter type and number of poles. To meet the specifications in Table I, the Type I filter was selected as a six-pole Butterworth design from the graph on Page 86, Reference 2 and the Type II filter from Page 88, Reference 1, which is a four-pole Chebyshev design.

A generalized filter consists of a number of resonant sections (poles) coupled together and to the outside world in a specific way. These filters have been implemented with a variety of resonant elements, including mechanical, electrical, electromechanical, and piezoelectric. One method of modeling such filters is to use an equivalent electrical network [1,2,4] and relate the electrical parameters to the appropriate filter elements, in this case SAW transducers and grating reflectors. This is the approach followed by Matthaei[5] and is the design technique used here. Rosenberg and Coldren[6] use a similar approach where the filter elements are translated in SAW elements and analyzed via a scattering matrix formalism. While both design techniques offer considerable power and versatility and are necessary for the initial design, they do not easily handle the complexity and precision required in the fabrication of multipole filters[7]. To do this, a building-block approach[8,9] which has been used successfully in the production of bulk wave crystal filters has been adopted and is treated in detail in Section 3.

2.2 TYPE I FILTER DESIGN

Before Matthaei's[5] approach can be used to synthesize the six-pole filter, the following acoustic parameters must be chosen. Of the various coupling schemes--acoustic, multistrip coupler, transducer and evanescent--a combination of acoustic and transducer coupling was chosen as they were the best developed techniques, were consistent with the building-block approach, and met the filter specifications. The combination of coupling schemes used affects the filter out-of-band rejection level, which is defined as the difference between the passband attenuation and highest sidelobe level. Theoretically, a minimum of two sets of transducer-coupled cavities are required to yield 60 dB of rejection. Acoustic coupling, though it is very economonical of crystal area, does not yield high sidelobe rejection levels, so is used with transducer coupled cavities. The six-pole Type I filter, requiring five coupled cavity-pair, was designed to have two transducer couplings and three reflector coupled pair as illustrated in Figure 2 and the four-pole Chebyshev design in Figure 1 .

The next step in synthesis was to select the groove-depth/ metal-thickness and the reflector length (not the coupling reflectors which are sized later) for the system. The considerations here are: 1) to minimize the reflector length to keep the overall device size down especially in the VHF frequency range, and 2) to use as shallow a groove depth as possible to maximize the cavity Q and allow for a wider acoustic aperture. These are conflicting requirements which we resolved by calculating the cavity Q[10] for a range of depths and relector lengths. For the Type I filters we chose $h/\lambda_0 = .01$ and 1000 grooves based on data in Table II. The last 200 grooves of each reflector were cosine weighted to reduce the coherent out-of-band reflection from the reflector ends. Figure 3 shows the out-of-band response from one two-pole section. The small out-of-band ripple is due to the reflector weighting.

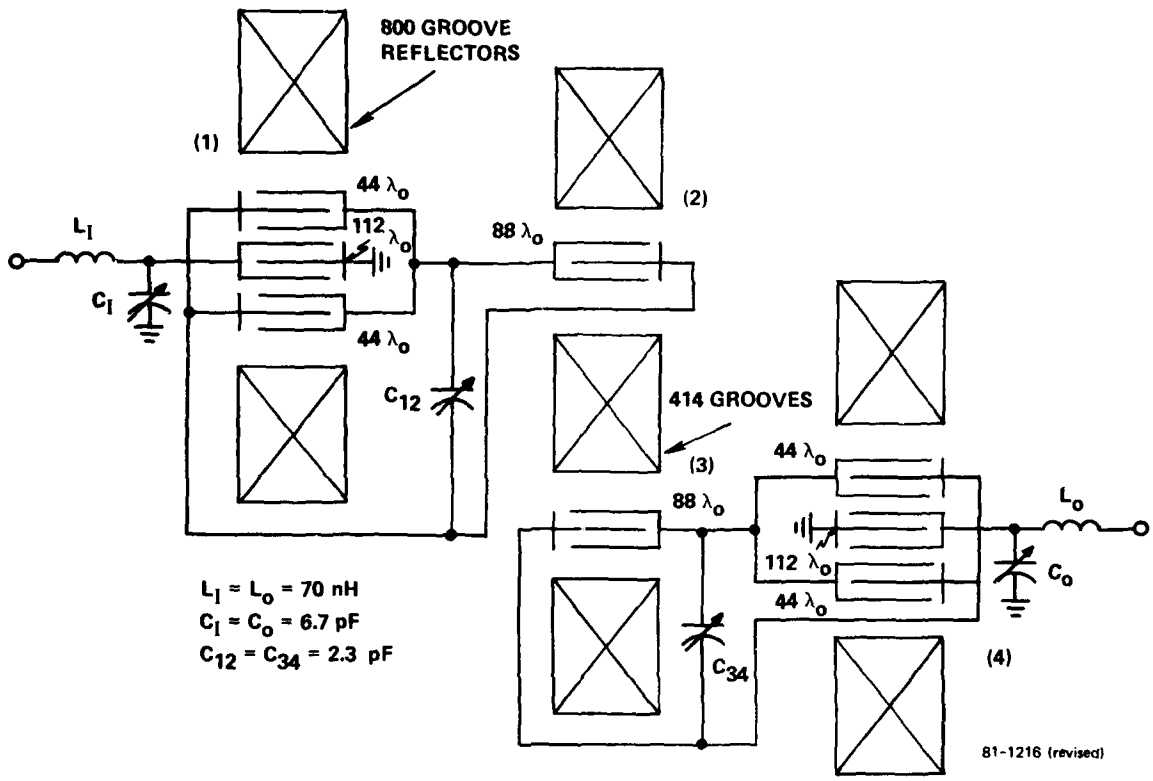

FIG. 1 Schematic showing the four-pole configuration with two transducer-coupled cavity-pairs and one pair coupled by a reflector. Component values shown are for the Type II filters.

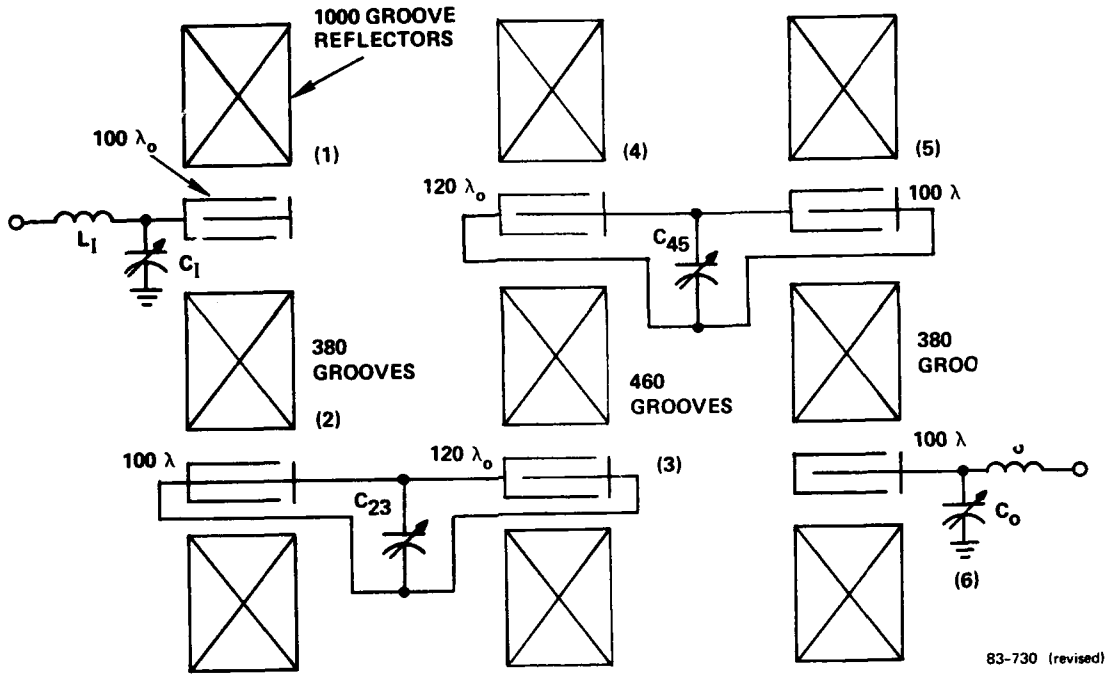

$L_I = L_o = 75$ nH $\quad C_{23} = C_{45} = 2$ pF
$C_I = C_o = 4.9$ pF

FIG. 2 Schematic showing the six-pole configuration with two transducer-coupled cavity pairs and three pair, coupled acoustically. Component values shown are for the Type I filters.

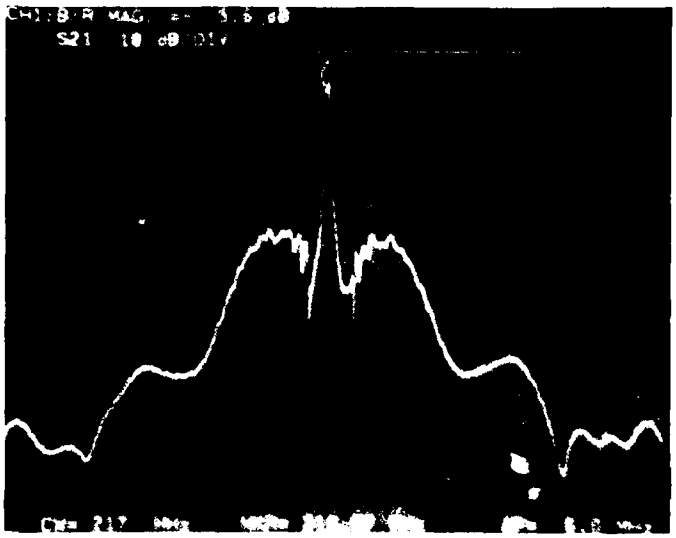

83-731

FIG. 3 Out-of-band rejection of one two-pole section with cosine weighting of reflector ends and cosine weighted transducers.

TABLE II

Cavity Q's (Units of 1000) for Various Depth (h/λ_0) and Reflector Lengths (Ng) for Type II Filters

depth/wavelength ratio h/λ_0	Number of reflector grooves (Ng) 700	800	900	1000	1100	1200
.006	22	32.2	42.5	51.4	58.1	62.6
.008	43.1	54.0	61.0	64.8	66.6	67.5
.010	53.0	63.4	65.6	66.5	66.8	66.9
.012	62.9	64.7	65.2	65.4	65.4	65.4
.014	63.0	63.5	63.6	63.6	63.7	63.7

The acoustic aperture is dependent on the groove depth in the reflectors and on the transducer apodization; and is limited by the onset of higher order transverse modes[11,12] in the resonant cavity. In general the wider the aperture the more flexibility there is in designing the transducer. For this design an aperture of 44 λ_0 (where λ_0 is the acoustic wavelength) was experimentally determined to be the widest practical before the onset of transverse modes.

Temperature performance of the available SAW materials limit the material selection to ST Quartz[16] or a related rotated Y cut. ST cut was used before.

The material parameters such as velocity, capacitance, and electro-acoustic coupling constant (k^2) had to be ascertained for use in the synthesis routine. Previous experimental work determined the velocity in the reflectors as a function of groove depth[13] and in the recessed transducer[11]. The free surface velocity was also found[13] to agree with calculation at a value of 3157.6 ± 0.2 m/sec. These velocities are required in the analysis routines to establish the period for the transducers and reflectors, and the gaps in the cavities in order to attain the desired resonance frequencies. In spite of this effort it was still necessary to trim[17] the cavity frequencies following device fabrication. The capacitance

per meter on ST quartz for quarter-wave electrodes on half-wavelength centers is well established to c_1 = 25.2 pF/m. For the initial designs we used k^2 = .0016 which is based on experimental data[15]. Although there are slight changes in the values of k^2 and the capacitance due to the recessed structure[14] which have not been taken into account.

The Type II four-pole Chebyshev filter was used to illustrate Matthaei's synthesis procedure. We had to initially select transducer sizes, then synthesize the coupling reflector length and matching component values, analyze the design and iterate if required. As it turns out, iteration was required because we wished to have the coupling components between transducers to be capacitors (C_{12} and C_{34}) and the rejection level decreased to unacceptable levels for certain combinations of transducer lengths. The procedure begins by selecting the "low-pass prototype" element values (g_i's) tabulated in Ref. 14 for various filter types. For the four-pole 0.5 dB ripple Chebyshev (Type II) filter Table 4.05-2(a) of Ref. 14 yields the element values in Table III.

Table III

Lowpass Prototype Element Values for the Type II Filter

g_0	g_1	g_2	g_3	g_4	g_5
1.0	1.6703	1.1926	2.3661	0.8419	1.9841

The inverse filter Q, designated[2] as W, is given by (1).

$$W = \frac{\Delta F_3}{F_o} \qquad \frac{1}{Q_F} \tag{1}$$

where ΔF_3 is the filter bandwidth between the 3 dB points, F_o is the center frequency, and Q_F is the filter Q. The input/output electrical Q values Q_{E1} and Q_{E5} are defined by (2):

$$Q_{E1} = \frac{g_o \; g_1}{W} \quad ; \quad Q_{E5} = \frac{g_4 \; g_5}{W} \tag{2}$$

and the intercavity coupling constants $k_{j,j+1}$ are computed from (3).

$$k_{j,j+1} = \frac{W}{\sqrt{g_j \; g_{j+1}}} \tag{3}$$

The above expressions for Q_{Ej} and $k_{j,j+1}$ are from Table I Ref. 2 with W'_1 (of Ref. 2) set to unity. The expressions required to calculate other quantities are summarized below:

b_j - susceptance slope parameter for cavity j

$$b_j = b_{j-1,j} + \frac{M_j \pi}{2} + b_{j,j+1} \tag{4}$$

where M_j is the edge-to-edge cavity length in half-wavelengths, and $b_{j,k}$ is the slope parameter associated with a reflector array on one

side of the cavity. The quantity $b_{j,k}$ is calculated using Eq. 8 of Ref. 2 for each reflector using design value of groove number and etch depth (where $u = \varepsilon = 1 + 1/2 \ h/\lambda_0$ for grooves[3]).

$J_{j,j+1}$ - impedance inverter between cavities

$$J_{j,j+1} = k_{j,j+1} \sqrt{b_j \, b_{j+1}} \tag{5}$$

and for coupling reflector ($N_{j,j+1}$ grooves)

$$J_{j,j+1} = \frac{1}{U} \, N_{j,j+1} \tag{6}$$

Equation (5) above applies to any form of coupling (transducer and reflector) and we see that for reflectors we have two constraints determining the reflector length. In the design procedure we must therefore iterate, first selecting a coupling-reflector length (Ng) calculating J from (6) and comparing it with the J value from (5), which is itself a function of Ng. Fortunately, the J value from (5) is a slowly varying function of Ng (through the b_j value) and only one iteration is usually required. Since the procedure for synthesis is slightly intricate and somewhat confusing, we now simply tabulate various parameters used, to illustrate the technique.

Table IV

Type II Filter Parameter Values in Synthesis

N_p	88	112	(No. of transducer wavelengths.)
C_T	2.8428 pF	3.6182 pF	(total transducer capacitance x $2/\pi$ to account for cosine weighting)
$4/\pi\ k^2\ N_p$	.1793	.2281	
G_o	4.804×10^{-4}	7.778×10^{-4}	$G_o = 4/\pi\ k^2\ N_p \omega_o C_T$ (ω_o = radian frequency = $2\pi F_o$)
J_T	.03099	.03944	$\sqrt{2G_o}$ - transducer impedance inverter parameter
G_j		.1372	$G_j = g_j/Q_{Ej}$ (input/output transducer admittance-before inversion)
G_{xj}		.01134	J_T^2/G_L (inverted transducer admittance)
R_{pj}		88.202	$R_{pj} = 1/G_{xj}$ (transducer parallel resistance)

The parameters G_j, G_{xj}, and R_{pj} are calculated only for the input/output transducers, which referring to Figure have $N_p = 112$ wavelengths.

Table V
Type II Filter Additional Parameter Values
($Ng = 414$, $h/\lambda_0 = .012$)

	j	g_j		k_{ij}		$J_{j,j+1}$	b_j		$\Delta M_{cj}(\lambda_0)$
input	0	1							
cavity numbers	1	1.607					927.8		
			12	1.748×10^{-4}	12	.12756		12	.02030
	2	1.1920					574		
			23	1.4688×10^{-4}	23	.08431			
	3	2.3661					574		
			34	1.7477×10^{-4}	34	.12754		34	.02030
	4	.8419					9278		
output	5	1.98411							

The parameter ΔM_{cj}, given by (7), is the cavity length correction required to compensate for loading effects of one cavity on another.

$$\Delta M_{cj} = = \frac{|J_{j,j+1}|}{\pi} \quad \frac{\lambda_0}{2} \tag{7}$$

This correction is applied to cavities 2 and 3 only since the input/output impedance matching networks of Figure 1 perform this compensation for cavities 1 and 4. The value ΔM_{cj} is equivalent to a shift in resonance frequency downward since the cavity is being made longer, and here we see how simply Matthaei's approach yields this data. We now illustrate the procedure used to find Ng for the coupling reflector between cavities 2 and 3 (see Figure 1). Cavities 1 and 4 are $212\lambda_0$ long (total transducer lengths = 200 λ_0 plus four 3 λ_0 gaps) and the reflectors have 800 grooves .012 λ_0 deep. Thus the slope parameter for cavities 1 and 4 are

$$b_1 = b_4 = 130.88 + \frac{424\pi}{2} + 130.88 = 927.8$$

For cavities 2 and 3 we have an 88 λ_0 transducer plus two 6 λ_0 gaps for a cavity length of 100 λ_0. Thus the slope parameter for each is

$$b_2 = b_3 = 130.88 + \frac{200\lambda}{2} + x$$

where x is the slope parameter of the coupling reflector which we have yet to specify in length. Choosing Ng = 400 we find that x = 128.7 and $b_2 = b_3 = 573.74$. From (6), $J_{23} = .0914$ requiring that $b_2 = b_3 = 622.3$ which is larger than the value of 573.74. We have produced a Table of values for $J_{j,j+1}$ and $b_{j,j+1}$ for various reflector lengths (Ng) and etch depth (h/λ_0), which is reproduced as Appendix I. From this Table for r = 1.006 ($h/\lambda_0 = .012$) we find that $b_{j,j+1}$ varies very slowly while $J_{j,j+1}$ changes much more quickly. By increasing the value of Ng from 400 to 414, we change b_{23} from 128.71 to 129.04 and J_{23} goes down to .08401. The new value of $b_2 = b_3 = 573.82$ (very little change) while J_{23} from (5) is now .08428 which is close enough to .08401 (for Ng = 414) to be acceptable. Thus we see that only one iteration was necessary to find the $J_{j,j+1}$ values given in Table V.

The reflectors, transducers, and cavity length corrections have now been found and we must next determine the coupling capacitor value (C_{ij}) and the input/output matching circuit values. The first point to note here is that even though the values of g_j in Table V are nonsymmetric, the coupling values (J) and cavity corrections (ΔM) are very nearly symmetric and for all practical purposes we have a symmetric system. Thus, referring to Figure 1 , L_I, C_I and C_{12} are equal to L_o, C_o, and C_{34} respectively. The coupling capacitor (more properly a decoupling capacitor since it functions to decrease the inter-cavity transfer of energy) value is readily found from (8).

$$C_{j,j+1} = 2\,C_T \left[\frac{4k^2\,N_p}{\pi\,J_{j,j+1}} - 1 \right] \tag{8}$$

Thus utilizing the values for C_T and $J_{j,j+1}$ in Tables IV and V, we find that the required value of $C_{12} = C_{34} = 2.3$ pF. The input/output matching circuit values may be found, with reference to Figure 4, using the following procedure: (a) Calculate a value of C_p which, in parallel with C_T, will reduce the R_p to R_g when the parallel combination $(C_p + C_T + R_p)$ is changed to the equivalent series capacitance-resistance combination, (b) calculate a value of L which neutralizes the series equivalent capacitance found in (a). A simple sequence of formulae used to perform the above step is given below and the "cook-book"

$$X_T = \frac{1}{\omega_o\,C_T} \tag{9}$$

$$R_S = \frac{R_p\,X_T^2}{R_p^2 + X_T^2} \tag{10}$$

$$X_C = \frac{R_S}{\sqrt{\frac{R_S}{R_g} - 1}} = \frac{1}{\omega_o\,(C_T + C_p)} \tag{11a}$$

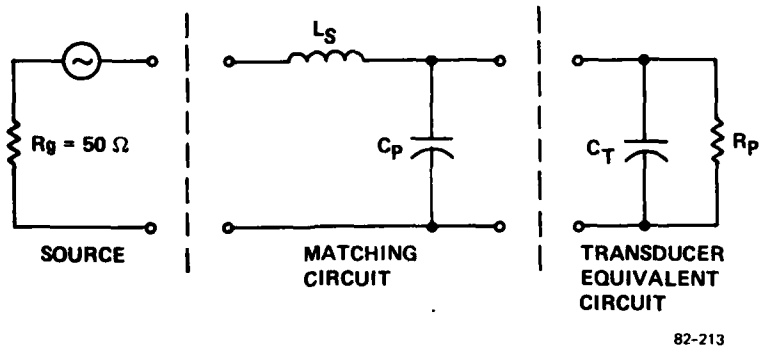

FIG. 4 Schematic diagram required to understand the matching circuit.

$$C_p = \frac{1}{\omega_o X_c} - C_T \tag{11b}$$

$$X_S = \frac{X_c R_p^2}{R_p^2 + X_c^2} = \omega_o L_s \tag{12}$$

procedure is to use the values of C_T, R_p and ω_o found earlier to calculate to C_p from (11b) and L_s from (12). This procedure is straightforward and accurate and the numbers are given in Table VI below:

Table VI

Matching Circuit Values Calculated for Type II

$\omega_o = 2\pi\ 150\text{x}10^6$	$X_T = 293.25$
$C_T = 3.618$ pF	$R_S = 80.88$
$R_p = 88.2$ pF	$X_p = 102.92$
	$C_p = 6.7$ pF
	$X_s = 43.58$
	$L_s = 46.24$ nh

This completes our descripton of the synthesis procedure and the illustration of this technique (Figure 1)

We now summarize this for the six-pole Type I filter which was fabricated and delivered to NRL. Performing an analysis, similar to that which resulted in Table II for Type II, we found that a relative groove depth (h/λ_o) of .01 and outside reflectors with 1000 grooves yielded the optimum cavity Q value. Since the Type I filter resonance frequency is 217 MHz and the wavelength is commensurately shorter than the 150 MHz Type II design, the 1000 groove reflector yields a device which is well within overall length constraints. For this etch-depth the velocities[3,9] in both the reflectors and recessed transducers is about

3154 m/sec and this is the value used in the analysis to establish the wavelength. The configuration of Figure 2 was selected as being most economical in space and yielding an acceptable (theoretically) level of rejection. We used an aperture of $44\lambda_0$ and cosine-weighted symmetrically located transducers. For the six-pole Butterworth response (Type I) filters, Table 4.05-1(a) of Ref. 14 gives the required low-pass prototype element values listed below in Table VII. We note first of all that the values of g_j are symmetric and this results from the fact that the filter is a lossless-Butterworth design. We compare this symmetry with the asymmetry of the even-order Chebyshev design. Odd-order lossless Chebyshev designs are exactly symmetric. When losses are included, all designs become asymmetric[6].

Table VII

Type I Filter - Design Parameter Values for Synthesis

	j	g_j		k_{ij}		$J_{j,j+1}$	b_j
input	0	1.0			01	.0068	
cavity number	1	.5176	12	2.154×10^{-4}	12	.1500	621
	2	1.414	23	1.115×10^{-4}	23	.0068	621
	3	1.932	34	0.9534	34	.1008	688
	4	1.932	45	1.115×10^{-4}	45	.0068	688
	5	1.414	56	2.154×10^{-4}	56	.1500	621
	6	.5176			67	.0068	621
output	7	1.0					

N_p	C_T	$4/\pi k^2 N_p$	G_o	J_T	G_j	G_{xj}	R_{pj}
100	2.235	.20375	6.207×10^4	.03524	.2351	.00528	189

In this design we chose to make middle section transducers $120\lambda_o$ in length and the input/output ones $100\lambda_o$, with $3\lambda_o$ gaps, since adjustments in coupling could be effected by varying the length of the coupling reflectors and the matching/coupling component values. We believed that $N_p = 100$, 120 would result in (de)-coupling capacitor (C_{23} and C_{45} of Figure 2) values which were manageable, that is, not being too small and subject to being overpowered by parasitic capacitances. The calculations required to find the coupling reflector lengths, input/output matching circuit values, and coupling capacitor value were then found as described earlier for Type II and these values are shown in Figure 2 .

2.3 ANALYSIS

Following synthesis, we analyzed each design to see how well the synthesis procedure worked. We found that the procedure worked very well, and that only a few minor adjustments (coupling or matching component values) were required to achieve a computed response which we considered satisfactory. Perfection was, in general, not possible due to the losses included in our analysis and the large number of parameters which could be in error and adjusted. From the analysis, we also determined the exact frequencies to which each cavity (when isolated) must be set to achieve the response desired, and the required transmission response of each reflector-coupled cavity-pair. During fabrication we then knew where to set the cavity frequencies and how to adjust coupling-reflector coupling strength.

We had a number of computer routines, developed for internal use though during our previous work with resonators, which allowed us to analyze resonators with various combination of reflectors and transducers. The routines utilize the Mason equivalent circuit model[18] (cross-field) with viscous, air, and bulk mode losses, and electrical feedthrough included. The calculations for an N element reflector or transducer are made in closed form using the matrix techniques developed by Field, Ho and Chen[19]. In this technique, we calculate the appropriate matrix elements for a single "cell", consisting of a complete reflector or transducer segment, and then raising this matrix to the Nth power we obtain the matrix for an N element array. This makes N matrix-multiplications unnecessary and reduces the computation time by orders of magnitude since N can be as high as a thousand. The single limitaton on this technique is that one cannot model weighted transducers or reflectors. We must revert to previously developed routines, which take much more computer time, to model weighted structures. In the model, we can also vary the velocity directly or by adding reactances[20] at the element edges.

In order to model the structures used in this program, we had to develop routines which would allow us to cascade various acoustic strutures such as we show in Figures 1 and 2 with variable matching/coupling networks. The scheme which we adopted is illustrated in Figure 5 . For each of M frequencies the ABCD matrix is computed and stored for an acoustic structure (two-port single-pole resonators, or two-pole acoustically-coupled resonator). The coupling/matching network configuration is then defined and the ABCD matrix for the entire structure is computed. From this complete ABCD matrix, all the interesting electrical parameters of the filter are determined and plotted. Since recomputing the complete matrix is very rapid when only the coupling networks are changed, this procedure is extremely efficient and allows us to analyze and tweek the various configurations in a short period of time.

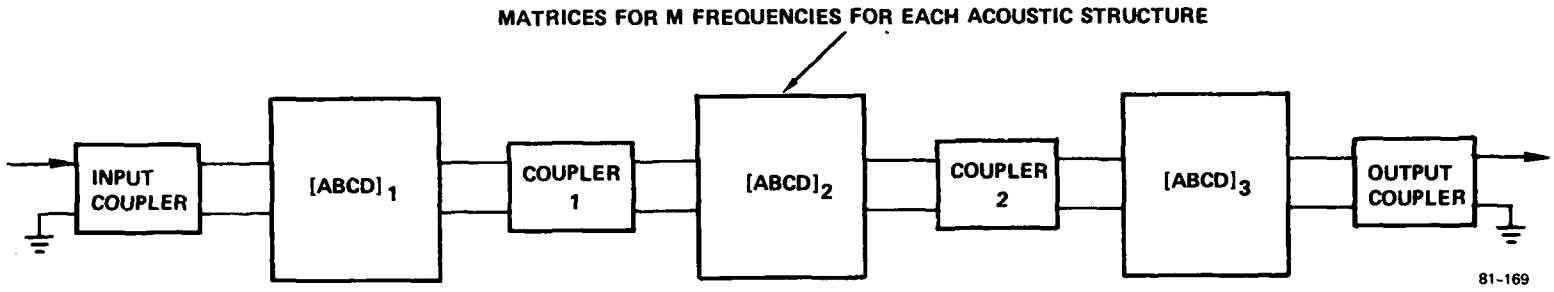

FIG. 5 Schematic representation of our scheme for efficient computation of the response of a multipole filter. Coupler matrices are recomputed as these components are varied for each of the M frequencies.

We now present the results of calculations for Type II followed by similar results for Type I. In Figures 6, 7, and 8 we show the filter response, for varying bandwidths, for the structure of Figure 1 . These results are computed for a device with no air loading since the device will ultimately be sealed in a vacuum. We note the salient features of the computed response and compare these with the specifications (of Table I) in Table VIII. First of all, we did not achieve the Chebyshev bandpass (with three dips for a four-pole). A review of the literature indicates that it is frequently very difficult to achieve the theoretical passband response and our experience bears this out. Rather than spend a

Table VIII

Desired and Predicted Response for Type II

	Desired	Predicted
Loss	6 dB max	2.1 dB
ΔF_3	37 kHz min	47 kHz
Shape Factor (60/3dB)	8.1	5.2
Response Shape	Chebyshev (3 dips - 0.5dB)	Single Dip (0.5dB)
Minimum Rejection at		
$F_R \pm 0.15$ MHz	60 dB	66 dB
$F_R \pm 0.5$ MHz	80 dB	60 dB
$F_R \pm 5.0$ MHz	110 dB	135 dB

lot of time tweeking the design to produce the 3-dip response we accepted the response of Figure 8. Secondly, we see that the 3 dB bandwidth is wider than required and that the shape factor is smaller than specified, both characteristics being favorable. The predicted loss of 2.1 dB is well under required 6 dB, leaving significant room for unaccounted for losses and errors. Since the shape factor was low (which is good) it is no surprise the find that the rejection at $F_0 \pm 0.15$ MHz exceeds the

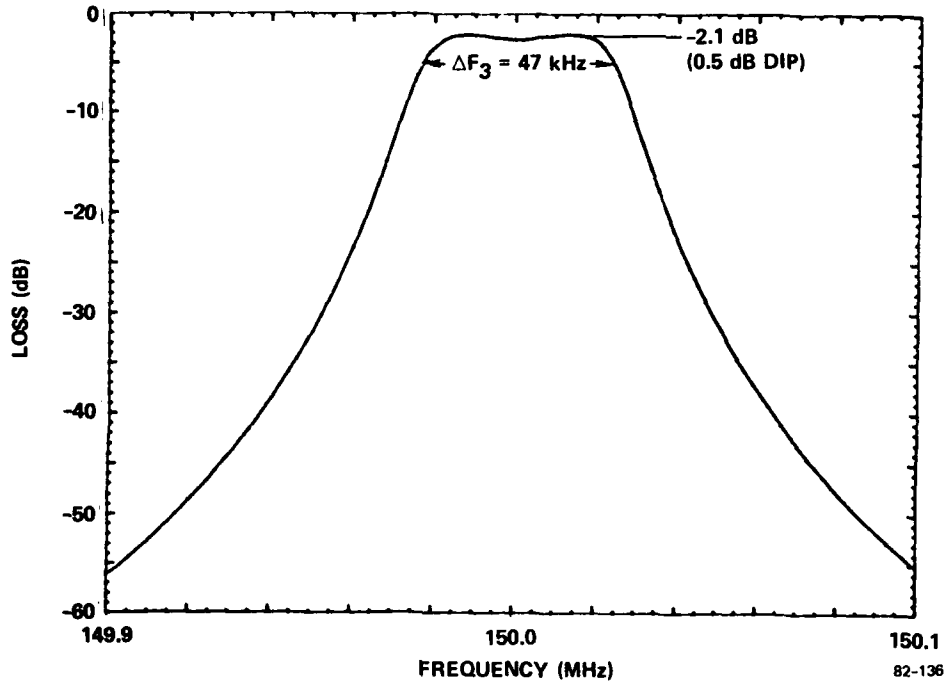

FIG. 6 Computed narrowband response for Type II with component values as given on Fig. 1.

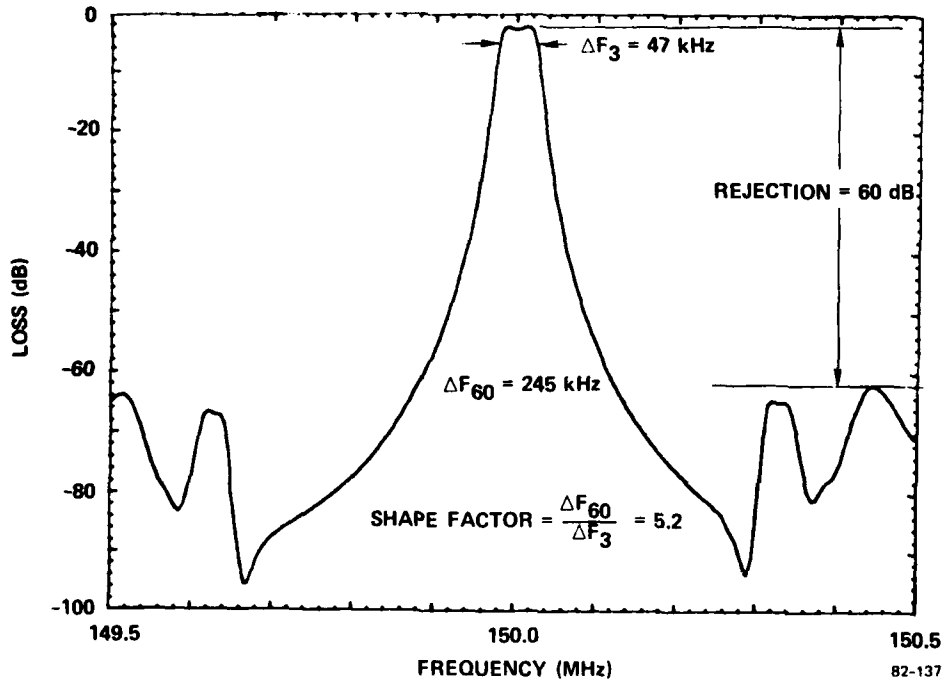

FIG. 7 Computed response for Type II with component values as given on Fig. 1.

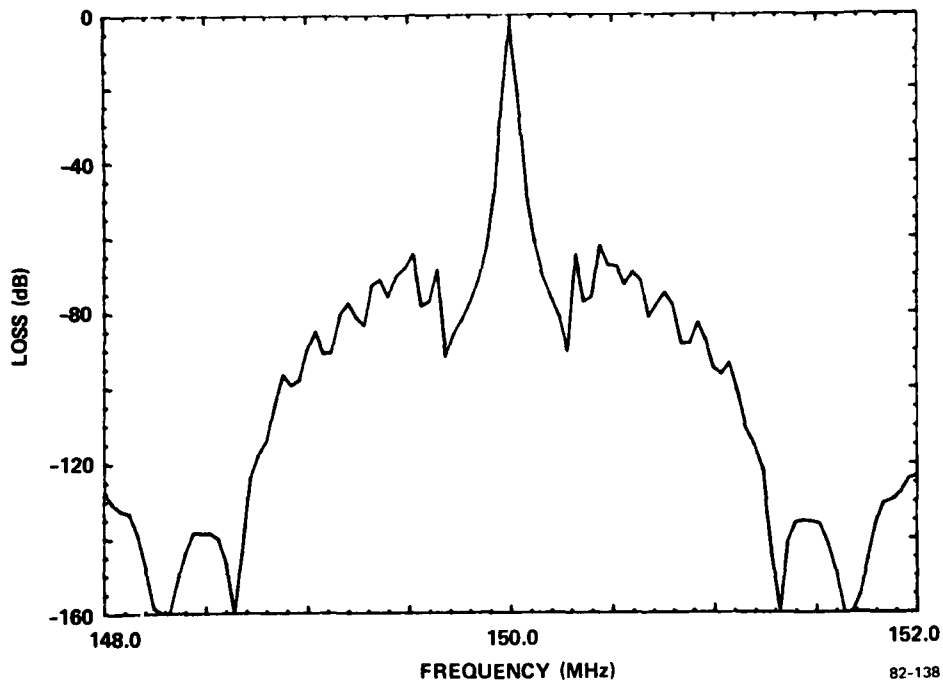

FIG. 8 Computed wideband response for Type II with component values as given in Fig. 1. Note that the acoustic response is down 110 dB at $F_o \pm 1.1$ MHz.

required 60 dB. However, at 0.5 MHz effect the rejection is much poorer than desired (60 vs. 80 dB) due partly to the reflector-sidelobe ripple but more importantly to the basic non-resonant response of the transducers. Further, this non-resonant response of Figures 7 and 8 is in error since the transducers are not apodized in the model but they are in the device. We shall see in the presentation of the experimental results that we indeed did not achieve the desired rejection level and these computer results show that a re-evaluation of the configuration, or a substantial redesign of the exiting configuration is necessary.

Further computed results are shown in Figure 9 where the VSWR (of the passband) is given, and in Figure 10 where the Smith chart plot of the input (and output since they are the same) impedance is shown. Further improvement (increased linearity in VSWR) in those characteristics can only be achieved by modifying the passband response. In Figure 11 we show the response of the acoustically-coupled pair (two-pole) consisting of cavities 2 and 3 of Figure 1 . When fabricating the device we endeavor to replicate this response experimentally by first setting the cavity frequencies and then the coupling strength (through the reflector) using our frequency-trimming and coupler-trimming techniques. In Figure 12 we show the computed electrical reflection coefficient magnitude, $/\Gamma/$, for cavities No. 2 (or 3 as they are the same in all respects for Type II) with the transducer in the opposite cavity open circuited, electrically unloading that cavity. The reason for computing $/\Gamma/$ (and measuring it) in this manner is that we obtain a dominant resonance (seen at the lower frequency ~ 149.96 MHz of Figure 12) which we can conveniently measure and adjust. When both cavities of an acoutically-coupled pair are not on the same frequency, which is generally the case as fabricated, it is very difficult, if not impossible, to adjust each frequency correctly with the other cavity loaded due to the coupling effects. In Figure 13 we show the computed response for the two-port cavities (1) or (4) for Type II. From this curve we find the resonance frequency to which these cavities must be trimmed in order to obtain the

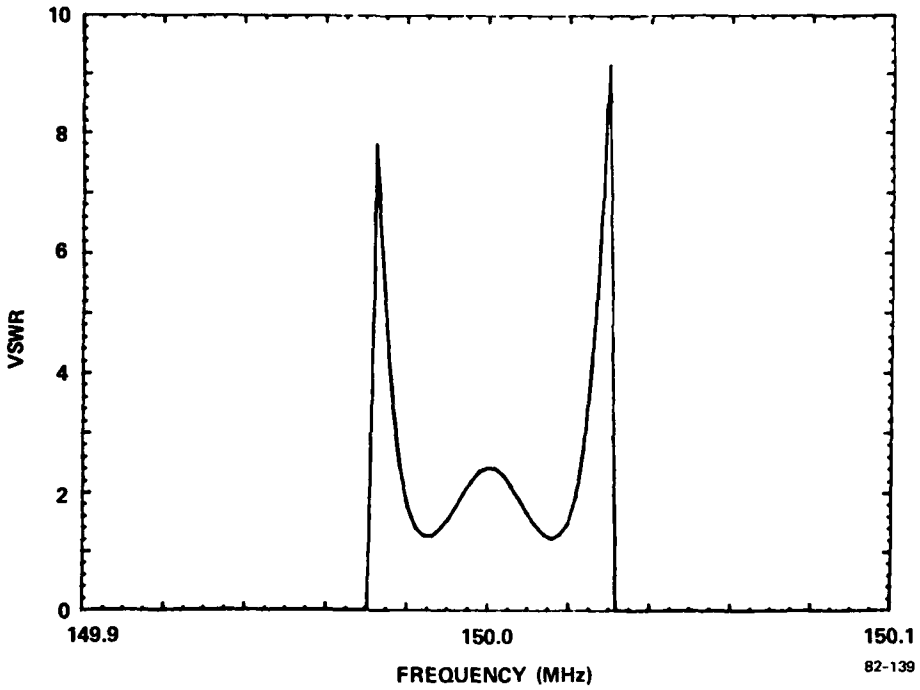

FIG. 9 Voltage standing wave ratio (VSWR) for Type II.

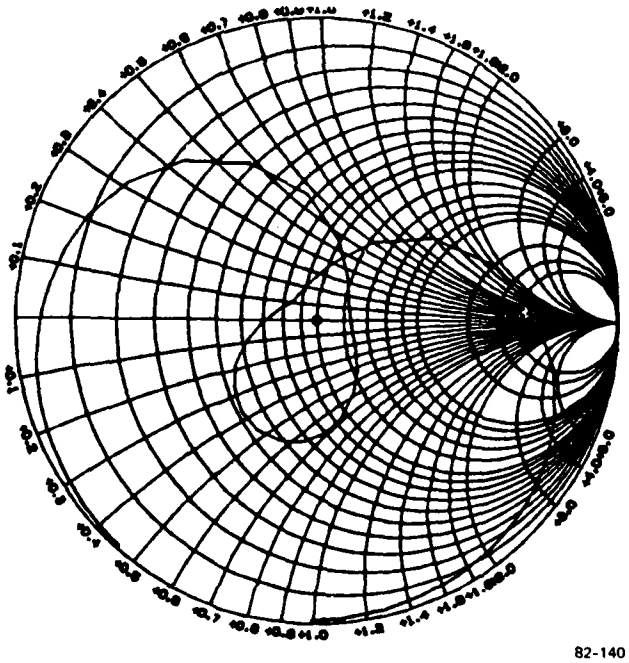

FIG. 10 Smith chart plot of the input (and output) impedances for Type II as shown on Fig. 1. The total bandwidth is 200 kHz.

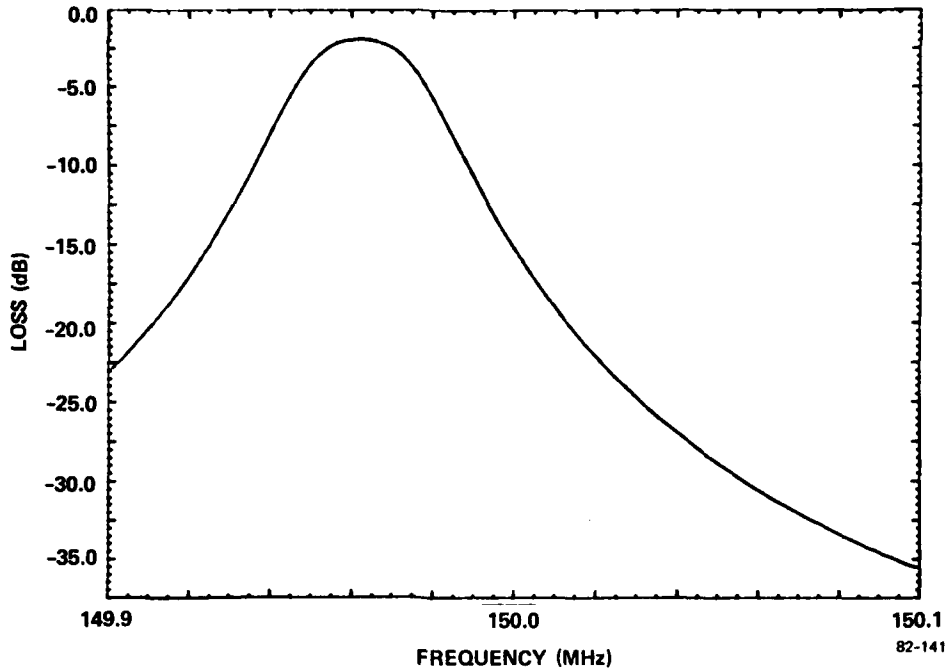

FIG. 11 Computed response of the acoustically-coupled cavity-pair for Type II (central portion of Fig. 1) unmatched.

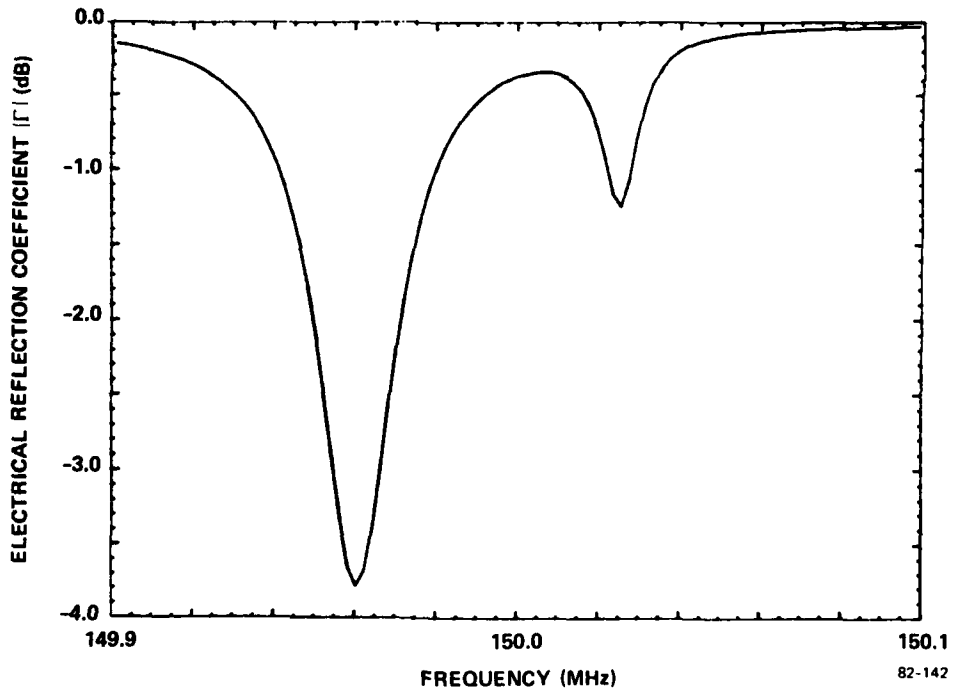

FIG. 12 Computed reflection coefficient magnitude, / /, for cavity No. 2 of Type II (central section of Fig. 1) of the acoustically-coupled pair with cavity No. 3 electrically unloaded.

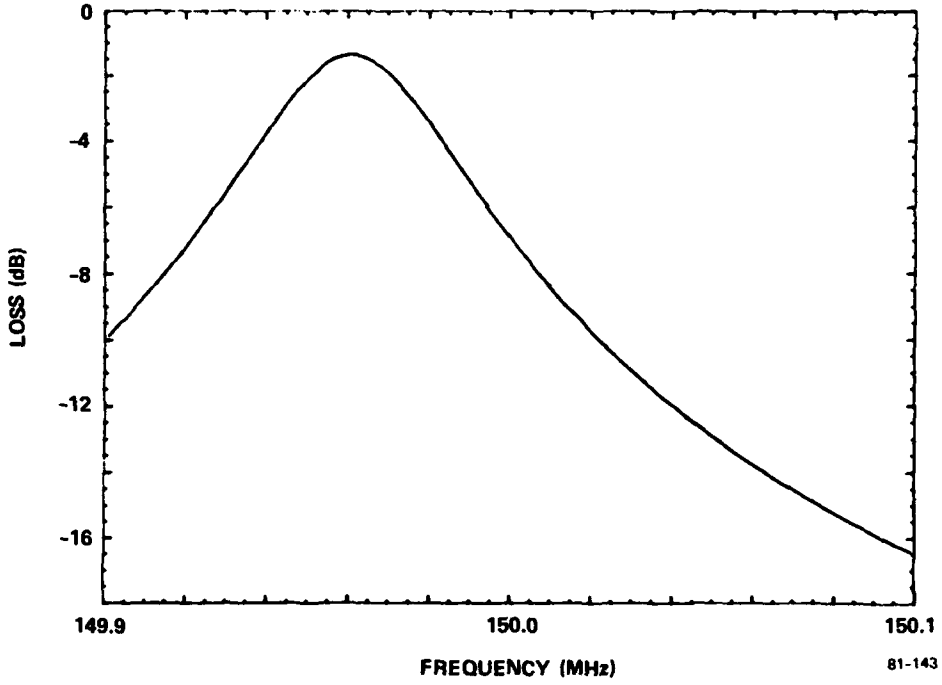

FIG. 13 Computed response for one of the two-port resonators of Type II (Fig. 1) unmatched into 50 ohms.

response of Figure 6. The calculations for Figures 6 through 13 were performed with air-losses included because the required measurements during fabrication are most conveniently done in air.

The question of how accurately we must set the cavity frequencies naturally arises and we have performed calculations showing that frequency errors on the order of 10 percent of the filter bandwidth have no appreciable effect on the filter response. For Type II this acceptable error is about 4 kHz, and we are experimentaly able to meet this requirement with no difficulty. The important measure of the error is its fraction of the center frequency (F_R). For example, 4 kHz at 150 MHz is about 25 parts-per-million (ppm) and we can readily trim to less than 10 ppm. Thus, narrow filter bandwidths or high frequency (> 600 MHz) could be significantly more difficult to make than the Type I and II filters in this program.

For the Type I filter Figures 14 through 23 show all the computed data necessary to assess the design and fabricate the devices. The salient aspects of the response are compared with the specifications in Table IX. We see that the design response exceeds all requirements by a significant

Table IX

Desired and Predicted Response for Type I

	Desired	Predicted
Loss	10 dB max	4.3 dB
ΔF_3	40 kHz	48 kHz
Shape Factor (60/3 dB)	4	3.5
Response Shape	Butterworth	Butterworth
Rejection outside:		
$F_R \pm 1$ MHz	60 dB	74 dB
$F_R \pm 2$ MHz		140 dB

amount which increases the probability of fabricating devices which meet specifications. The data of Figures 14 through 18 is self explanatory and shall not be discussed further. The response of Figure 19 is of interest since it shows the transmission response which we must have for cavities No. 1 and 2 (or No. 5 and 6) of Figure 2. Both of these cavities are to be trimmed to different frequencies as shown on Figures 20 and 21 where the cavity resonances for $/\Gamma/$ are shown. We note that Figure 19 has a large dip in the passband, which is due both to a high level of coupling and to the differing cavity resonance frequencies. For cavities No. 3 and 4, the resonance frequencies are to be the same (due to symmetry in the structure) at a value found on Figure 23, and the transmission response is as seen on Figure 22. The response of Figure 22 shows an almost critically coupled cavity-pair response which we must replicate experimentally. As with Type II, all responses are calculated with air losses included except the overall filter response, Figures 14-18.

While the Mason equivalent circuit approach is a useful design tool, it has not been developed to the point where it can accurately account for all the SAW resonator parameters. For example, the loss mechanisms in the resonator are many and are not sorted out in the model, the transverse modes are not included, and rectangularity of the groove shape is not dealt with. These short comings raise the problem that when the experimental results do not agree with the theory, which is often the case, it is difficult to feed the discrepancies back into the theory and obtain a meaningful result. The closing of this loop between the analysis and experiment remains an important objective in multipole filter technology. To circumvent this problem the experimental results of each building-block, a two-pole section, are fit to the standard lumped constant circuit (Figure 24), used for bulk-wave resonators. While this approach does not help to determine what went wrong, it does give a predictable procedure for adjusting and combining the SAW resonator sections as built. This is partcularly important for filters with a large number of poles and is treated in detail in the next section.

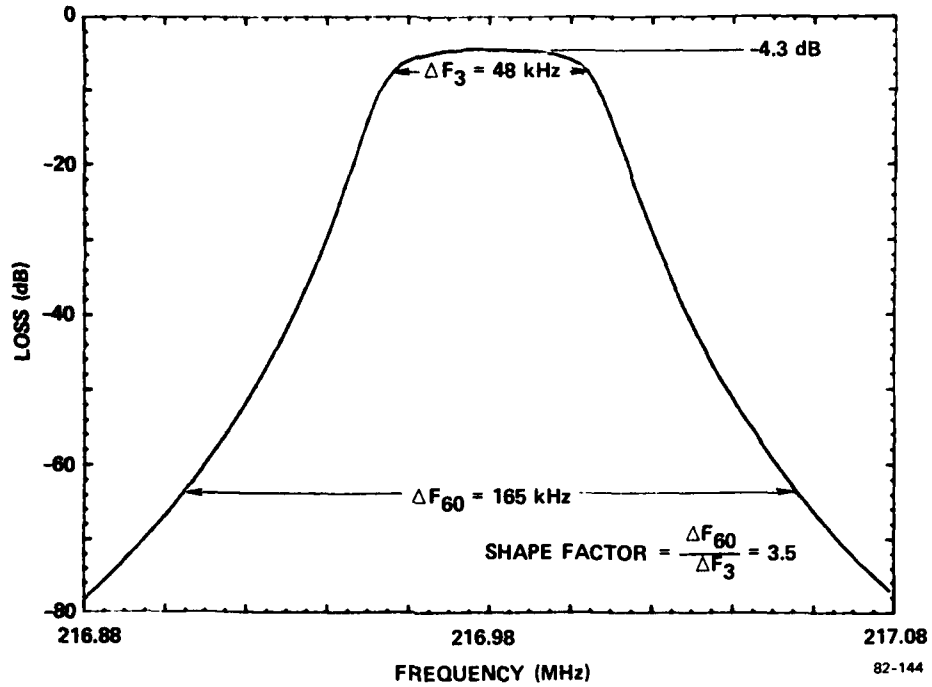

FIG. 14 Computed narrowband response for Type I with component values as given on Fig. 2.

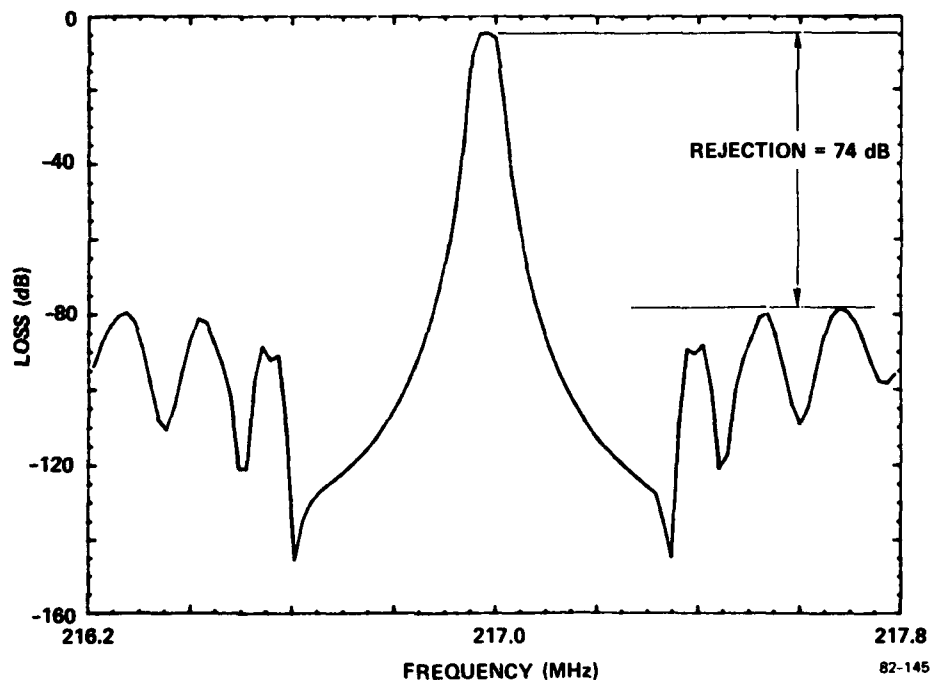

FIG. 15 Computed response for Type I with component values as shown on Fig. 1.

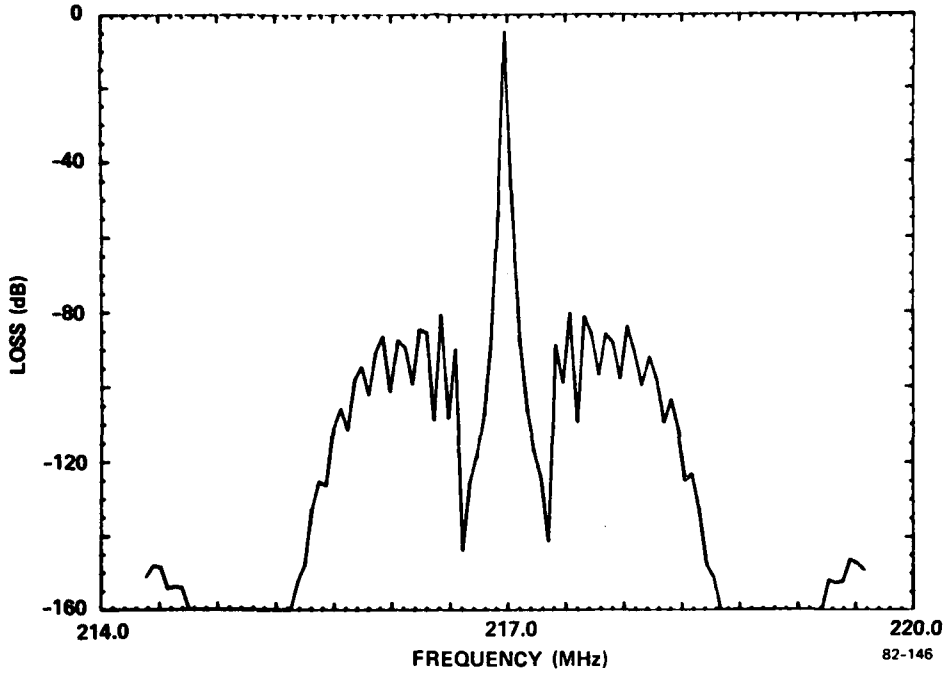

Fig. 16 Computed wideband response for Type I with component values as on Fig. 2.

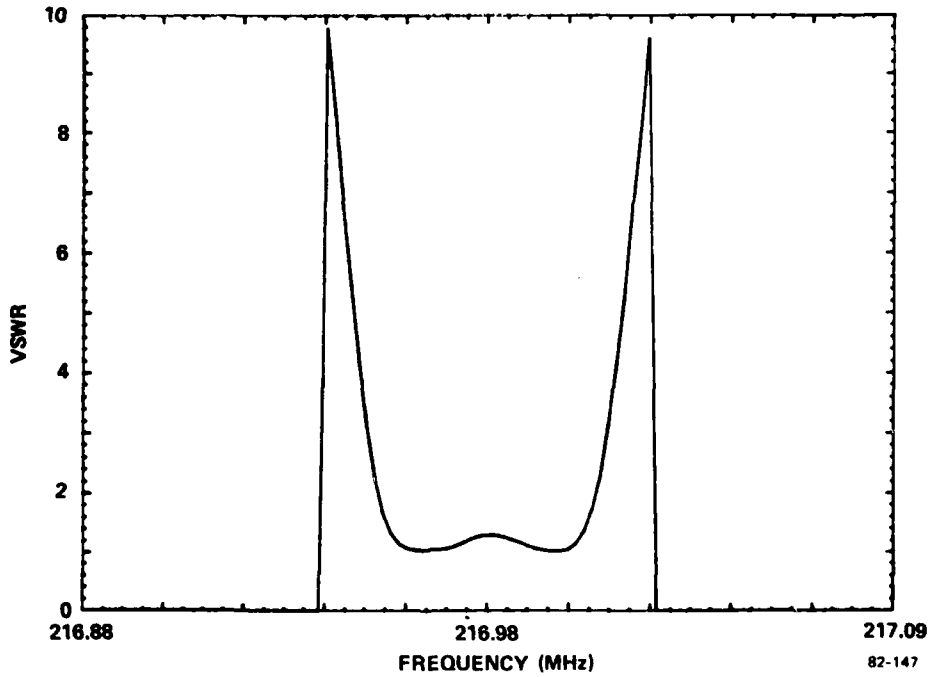

FIG. 17 Voltage stand wave ratio (VSWR) for Type I.

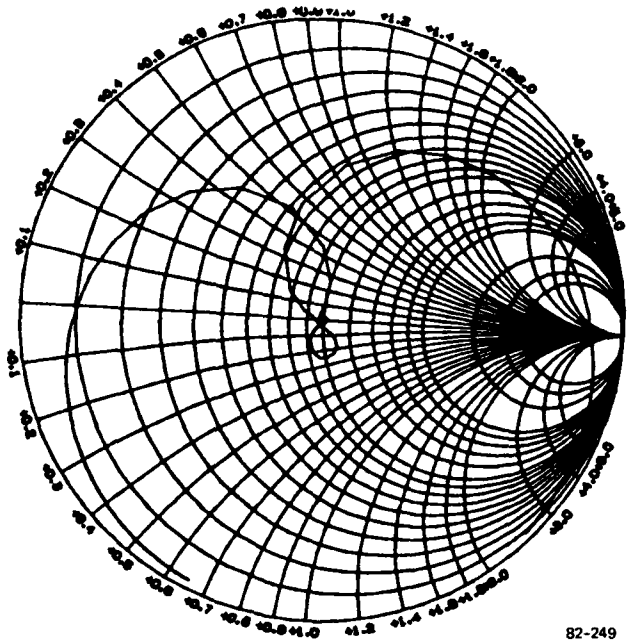

FIG. 18 Smith chart of the input (and output) impedances for Type I, as shown on Fig. 2. The total bandwidth is 200 kHz.

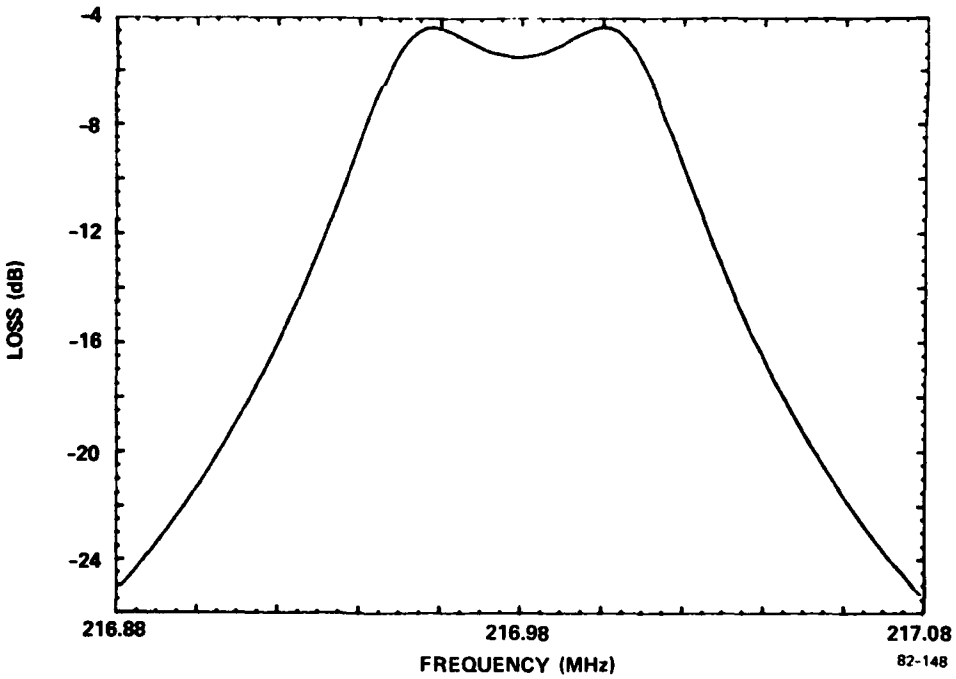

FIG. 19 Computed response of the acoustically-coupled cavities No. 1 and 2 (or 5 and 6) for Type I, electrically unmatched into 50 ohms.

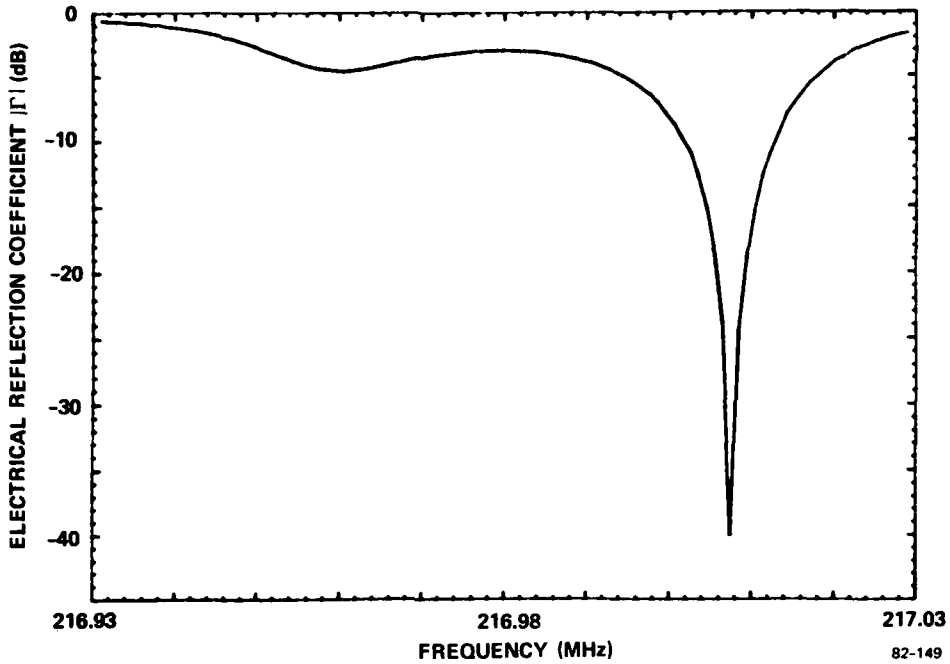

FIG. 20 Computed reflection coefficient magnitude, / /, for cavity No. 1 of Type I (the input in the upper left of Fig. 2) with cavity No. 2 electrically unloaded.

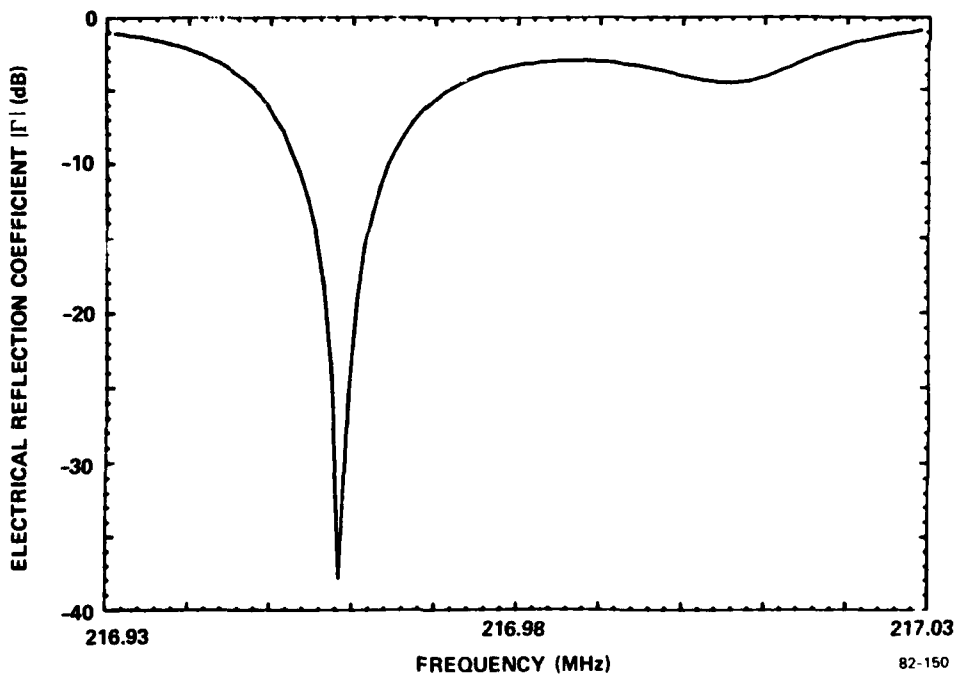

FIG. 21 Computed reflection coefficient magnitude, / /, for cavity No. 2 of Type I with cavity No. 1 electrically unloaded.

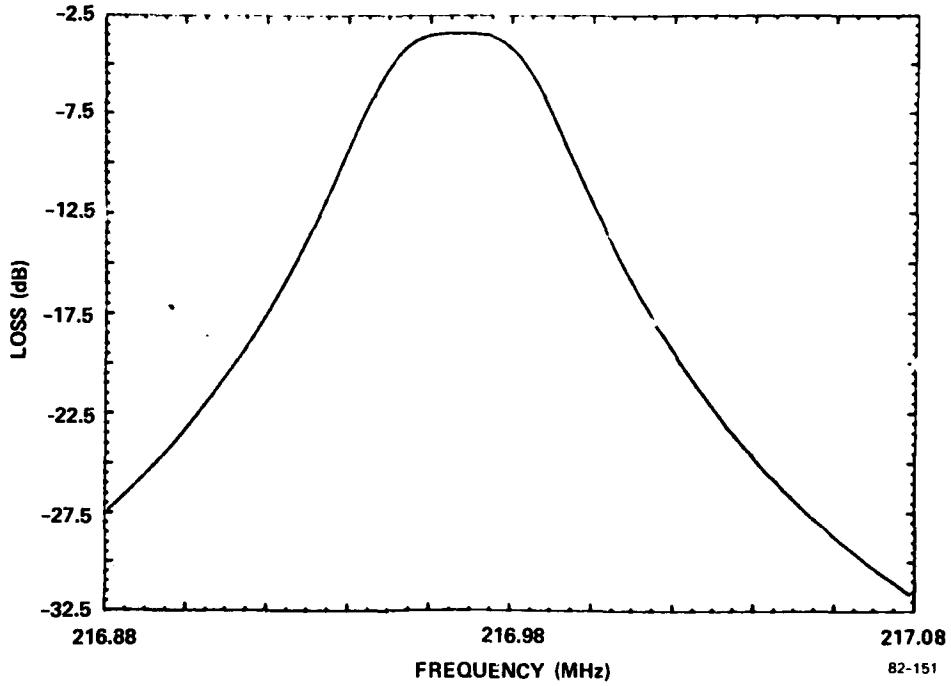

FIG. 22 Computed response of the acoustically-coupled cavity-pair (No. 3 and 4 of Fig. 2) for Type I, electrically unmatched.

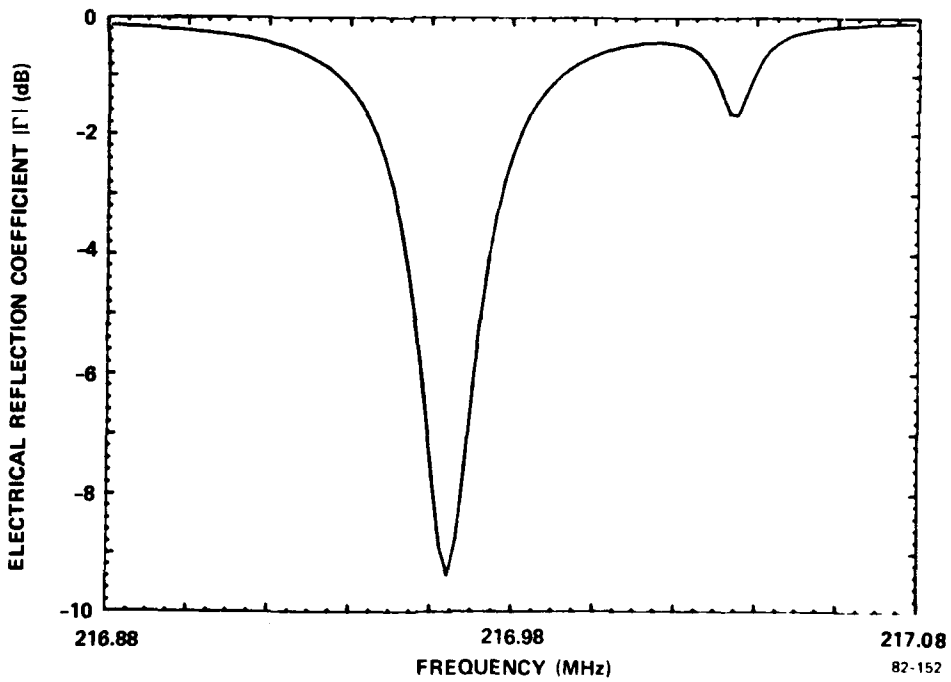

FIG. 23 Computed reflection coefficient magnitude, //, for Type I cavity No. 3 of Fig. 2 with cavity No. 4 electrically unloaded. Both cavities are the same frequency.

SECTION 3

MULTIPOLE RESONATOR FILTER MODELING

3.1 LUMPED ELEMENT MODEL

In this section, the method of modeling the two-pole sections, analyzing the designs and experimentally constructing a multipole filter based on theoretical guidelines will be described. The example of the six-pole filter will be used throughout the discussion, with the knowledge that the same procedures are applicable to any number of poles. Each step used in the actual analysis of the filter will be described in sequence, starting with the model for a two-pole section and leading to the complete six-pole filter.

An analysis approach based on an approximate lumped parameter model was selected because this approach gives the designer the most information and control at each step in the design. The complexity of the s-parameter of the admittance matrix approaches makes those inconvenient to use in the actual construction of the filters in the laboratory. The lumped elements model of the acoustically coupled section is based on a two-port resonator model by W.R. Shreve[21]. The two-pole model shown in Figure 24 is valid only near resonance and does not contain the necessary information about the out-of-band response of the SAW resonator filer. This circuit is idential to the well-established circuit representation of the two-pole monolithic crystal filter.

For a given resonator design, approximate values of the equivalent circuit elements can be found by using the relationships given in the following paragraphs.

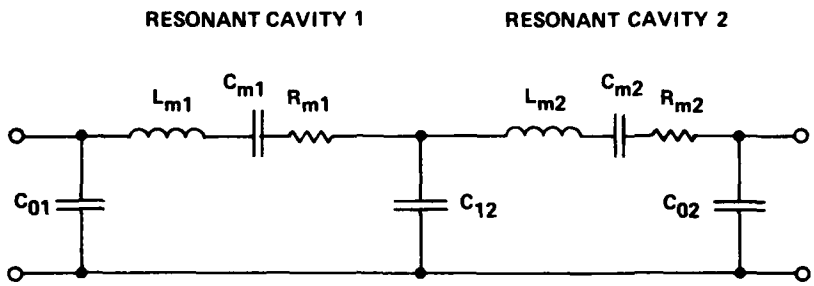

L_{m1}, L_{m2} : MOTIONAL INDUCTANCE FOR CAVITY 1 AND 2, RESPECTIVELY
C_{m1}, C_{m2} : MOTIONAL CAPACITANCE FOR CAVITY 1 AND 2, RESPECTIVELY
R_{m1}, R_{m2} : MOTIONAL RESISTANCE FOR CAVITY 1 AND 2, RESPECTIVELY
C_{01}, C_{02} : STATIC CAPACITANCE FOR THE IDT IN CAVITY 1 AND 2, RESPECTIVELY
C_{12} : COUPLING CAPACITANCE REPRESENTING THE ACOUSTIC COUPLING BETWEEN CAVITIES

83-698

FIG. 24 Equivalent circuit model of an acoustically coupled two-pole section.

The static capacitance of the transducer is given by:

$$C_o = N_e A C_i,$$

where,

N_e = the effective number of finger pairs (or, equivalently, the number of wavelengths) in the transducer.

A = transducer aperture (in meters).

C_i = the intrinsic capacitance per finger pair (in Farads/m).

For the type of cosine weighted transducers used in the designs for the current six-pole filter, $N_e = 2/\pi N$, where N = the actual number of finger pairs. For un-recessed transducers on ST-cut quartz, $C_i \approx 55$ pF/m, and for recessed transducers of the type used for this contract, $C_i \approx 69$ pF/m.

The acoustic resistance of the transducer is:

$$R_o = 1/(BK^2 f_o C_o N_e)$$

where

K^2 = piezoelectric coupling coefficient (for ST-cut quartz, $K^2 = 0.0016$)

f_o = resonance frequency (in Hertz)

and C_o and N_e are as defined above.

The motional inductance is given in terms of R_o:

$$L_m = \frac{m R_o}{4 f_o |\Gamma|} \cong \frac{m R_o}{4 f_o}$$

where

m = total cavity length in number of wavelengths.

The total cavity length $m = \ell + 2d$, where ℓ is the reflector edge to reflector edge cavity length and d is the distance from the reflector array edge to the effective center of reflection.

The motional capacitance can be calculated from the inductance by

$$c_m = \frac{1}{(2\pi f_o)^2 L_m}$$

The motional resistance

$$R_m = \frac{1 - |\Gamma|}{1 + |\Gamma|} R_o$$

Because the value of $|\Gamma|$ is not readily available, it is best to determine R_m experimentally. An approximate value of R_m for a given cavity can be obtained from the input impedance of the cavity with the second cavity unloaded. The value of the equivalent coupling capacitor is determined from the so-called "inverter parameter" $J = (1/r)^N$ where N is the number of reflectors in the coupling array and r is the reflection per reflector.

Then

$$X_{c_{12}} = J \frac{R_o}{2} ;$$

$$C_{12} = \frac{1}{\pi f_o J R_o} .$$

The equivalent values for the sections of the six-pole filter can now be calculated. For ease of analysis, measurement, and tuning, the two-pole sections were designed symmetrically; i.e., with both cavities having the same dimensions and the same transducers. In addition, due to the symmetry of the six-pole design itself, the input and the output section were designed differently. (For more detail regarding the design of the resonators themselves, please consult the relevant sections in this report.) The resulting equivalent circuit values are given below:

	Middle Section	Input/Output Section
IDT Length	120λ	100λ
IDT Aperture	44λ	44λ
Total Cavity Size	225λ	205λ
No. of Coupling Reflectors	460	380
C_o	3.4 pF	2.8 pF
C_m	1.5×10^{-3} pF	1.1×10^{-3} pF
C_{12}	10.5 pF	4.9 pF

These approximate values are used in a computer-based circuit analysis program. Two such programs were used. The first is COMPACT (by COMPACT Engineering, Inc.) available on the mainframe computer model Univac 1100/60 at Sperry Research Center. Then a second program by Hewlett-Packard, called the AC Circuit Analysis Program (AC C.A.P.) became available and was used for the remainder of the contract schedule.

Because this program is run on the desktop computer (Model HP 9836) which interfaces directly with the instruments used to measure the resonator filters, it was more convenient to use than COMPACT. The AC C.A.P. was modified to calculate and display reflection coefficient information identical to that obtained on the measurement setup.

The next step, then, is to calculate and plot the response curves corresponding to a particular design and to compare these curves with the measurements. (an example of these curves is shown in Figure 25 .) Due to the usual variations in the fabrication process, there are deviations from the design expectations. The values of the circuit elements in the model is modified so that the model agrees closely with the actual devices. A procedure was developed so that this process could be accomplished simply with a minimum number of measurements. First, from a representative wafer, a device which has equal pole frequencies, is selected for measurement (or if one is not available, a device can be trimmed in this fashion). Such a device has its input reflection coefficient dip frequencies equal to its output reflection coefficient dip frequencies. This property eliminates many of the complications from the modeling process and permits manual determination. The motional resistance R_m is determined by measuring the insertion loss and the input impedance at resonance (with the output port open-circuited). The measured results are compared with the corresponding circuit, and R_m is modified appropriately until both agree. The impedance of C_m at resonance determines the magnitude of the passband dip D as indicated in Figure 34. (If there is no dip as in the case of low coupling sections, passband shape or flatness can be used as a guide.) The coupling between the two poles, which is equal to C_m/C_o, determines the bandwidth, BW. The different parameters are interdependent to a certain extent. So, a few iterations may be necessary to achieve accurate circuit values. Obviously an efficient and precise method of determining the equivalent values would be to take the measurements automatically using the desktop instrument controller and then to optimize the values to fit the data. (Such a system was not developed due to scheduling limitations.)

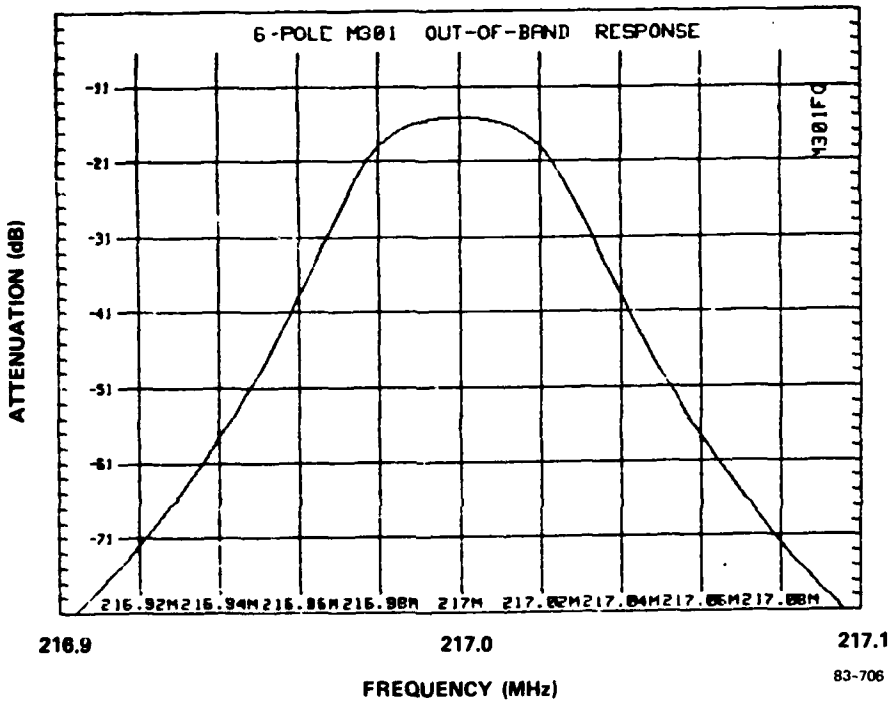

FIG. 25 Theoretical broadband attenuation characteristics of the six-pole filter (matched into 50 ohms) with resonator Q = ≅ 18,000 (in atmosphere). (Add 6 dB to all attenuation values to account for the way the program calculates attenuation.)

The parameter of major importance, the coupling, can be adjusted by changing the etch depth of the coupling array during or after fabrication. Thus if a device is found to have too much or too little coupling, another can be fabricated with the correct value.

Once the element values have been determined, the two-pole sections are used to design a six-pole filter following standard design procedures for coupled resonator filters. Such an approach is outlined in Humphreys[22]. Here a maximally flat (Butterworth) filter design based on infinite Q resonators was used. The major effect of having finite Q resonators is the added loss in the transmission band. Bandpass shape compensation for finite Q was not performed, but bandwidth narrowing due to finite Q was taken into consideration.

The circuit for a standard six-pole coupled resonator filter is shown in Figure 26. Using the values of C_{mi} (i = pole index) established previously, the coupling capacitance and source/load resistance values are given by:

$$c_{i,\ i+1} = \frac{f_o}{\Delta f\ k_{i,\ i+1}} \cdot \sqrt{C_{mi} \cdot C_{mi+1}}$$

$$R_s = \frac{\Delta f}{2\pi f_o^2 q_1 c_{m1}}$$

$$R_L = \frac{\Delta f}{2\pi f_o^2 q_6 C_{m6}}$$

(For the symmetric case, $R_s = R_L$) where $k_{i,\ i+1}$ are the normalized coupling values and q_1 and q_6 are the normalized q values for the desired (in this case, Butterworth) low-pass prototype filter. These values are available from standard design tables and are given below for the six-pole Butterworth prototype (these k values are normalized and are related to Matthaei's values by $l(\text{Matt}) = k(\text{norm})\frac{\Delta f}{f_o}$.

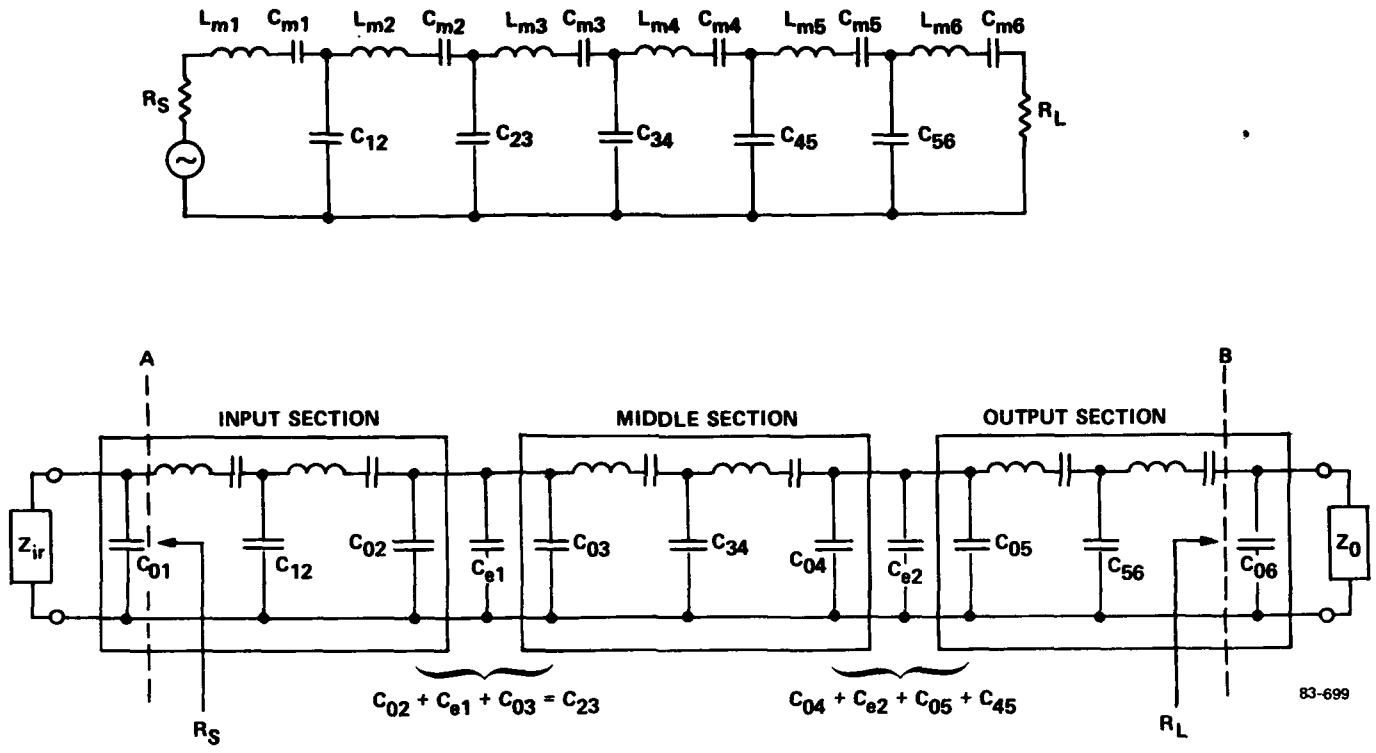

FIG. 26 Six-pole filter constructed of two-pole sections.

$$k_{12} = k_{56} = 1.1688$$

$$k_{23} = k_{45} = 0.605$$

$$k_{34} = 0.5176$$

$$q_1 = q_6 = 0.5176 \quad .$$

Because the coupling capacitors shift the resonance frequency of the poles, the pole frequencies must be adjusted so that when they are coupled, all poles will resonate at the same frequency, f_o. (This is called synchronous design.) The adjusted frequency for the ith pole, f_i, is given by:

$$f_i = f_o \quad 1 - \frac{C_{mi}}{2} \left(\frac{1}{C_{i-1,\ i}} + \frac{1}{C_{i,\ i+1}} \right) \quad .$$

Thus the motional inductance for the ith pole is

$$L_{mi} = 1/(2\pi f_i^2 C_{mi}) \quad .$$

The filter can now be constructed out of three two-pole sections as indicated in Figure 27 . The coupling capacitances C_{23} and C_{45} are obtained by adding external capacitances C_{e1} and C_{e2}, and taking into account the appropriate static capacitances (C_{oi}). Also, the input and output loading is now different due to the presence of C_{01} and C_{06}. This additional reactance must be accounted for in matching the circuit to the desired terminations (in this case, 50 ohms). The impedance at Point A and Point B in Figure 26 must be equal to R_L ($R_s = R_L$). This can be achieved by using a simple matching network which terminates in the desired 50-ohm impedance as indicated in Figure 27.

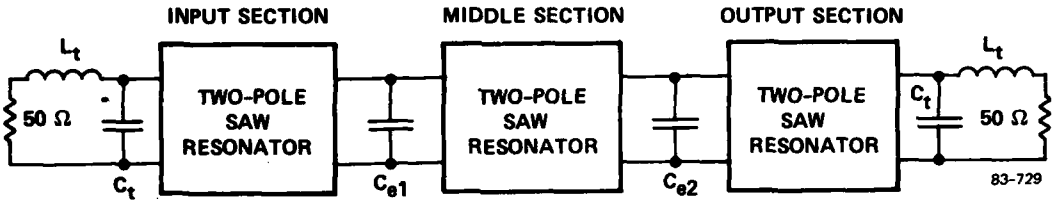

FIG. 27 Six-pole filter with input/output matching and 50-ohm terminations.

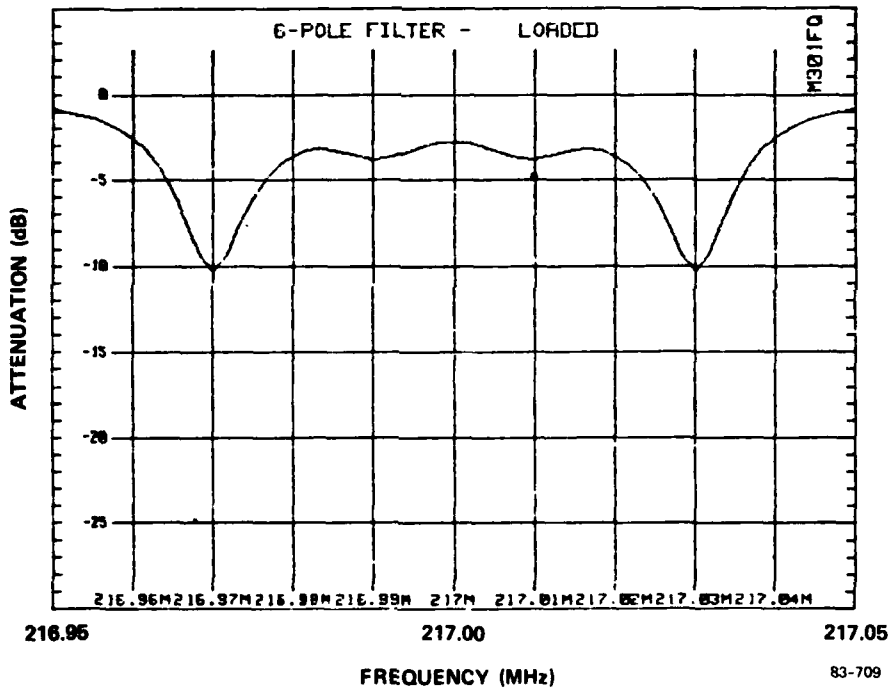

FIG. 28 Theoretical six-pole filter input reflection coefficient magnitude plot with both input and output loaded by 50 ohms and with no matching.

The matching network consists of a shunt capacitor C_t and a series inductor L_t. First, the series inductance needed to convert the 50-ohm series load into the equivalent resistance of R_L is found by:

$$L_t = \frac{1}{\omega_o} \sqrt{50\ (R_L - 50)} \quad , \qquad R_L > 50 \text{ ohms} .$$

Then this serices inductance is converted into an equivalent parallel inductance:

$$L_{parallel} = \frac{1}{\omega_o^{\ 2}} \cdot \frac{50\ R_L}{L_t} .$$

The total capacitance needed to resonate with $L_{parallel}$ leaving only the resistance R_L is:

$$C_{parallel} = \frac{1}{\omega_o^{\ 2}\ L_{parallel}} .$$

The capacitance C_t needed in the matching network is obtained by subtracting the static capacitance C_{01}, which is in parallel with C_t:

$$C_t = C_{parallel} - C_{01} .$$

If $C_{parallel}$ is less than C_{01}, then an inductor must be used. All of the above computation were performed using the desktop computer.

3.2 TYPE I FILTER MODEL RESULTS

The results for the six-pole filter are as follows:

f_o = 217.0 MHz (center frequency)
Δf = 26 kHz (compensation 3-dB bandwidth)
$R_s = R_L$ + 261.2 ohms (termination resistance)
$C_{m1} = C_{m2} = C_{m5} = C_{m6} = 1.15 \times 10^{-3}$ pF
$C_{m3} = C_{m4} = 1.46 \times 10^{-3}$ pF
$C_{12} = C_{56} = 4.64$ pF
$C_{23} = C_{45} = 10.1$ pF
$C_{34} = 13.3$ pF
$f_1 = f_6 = 216.973117$ MHz
$f_2 = f_5 = 216.960768$ MHz
$f_3 = f_4 = 216.972416$ MHz
$L_{m1} = L_{m6} = 467.875780$ μH
$L_{m3} = L_{m4} = 368.534674$ μH
$C_{e1} = C_{e1} = 3.89$ pF
$L_t = 75.4$ nH
$C_t = 2.94$ pF

Theoretical characteristics of the filter are shown in Figures 28, 29 and 30. The unmatched response is used for comparison to an actual six-pole filter during an intermediate stage in the construction; i.e., before final packaging. If the actual filter, Figure 31, is observed to agree with the predicted response with no matching, then final assembly is performed. Due to variations in the Q's of the actual devices, the insertion loss can vary about 1.5 dB in either direction.

Now that the six-pole filter circuit is designed and satisfies the desired characteristics, the two-pole sections that make up this filter can be individually analyzed. These sections directly correspond to the acoustically coupled two-pole SAW resonators. The measurements

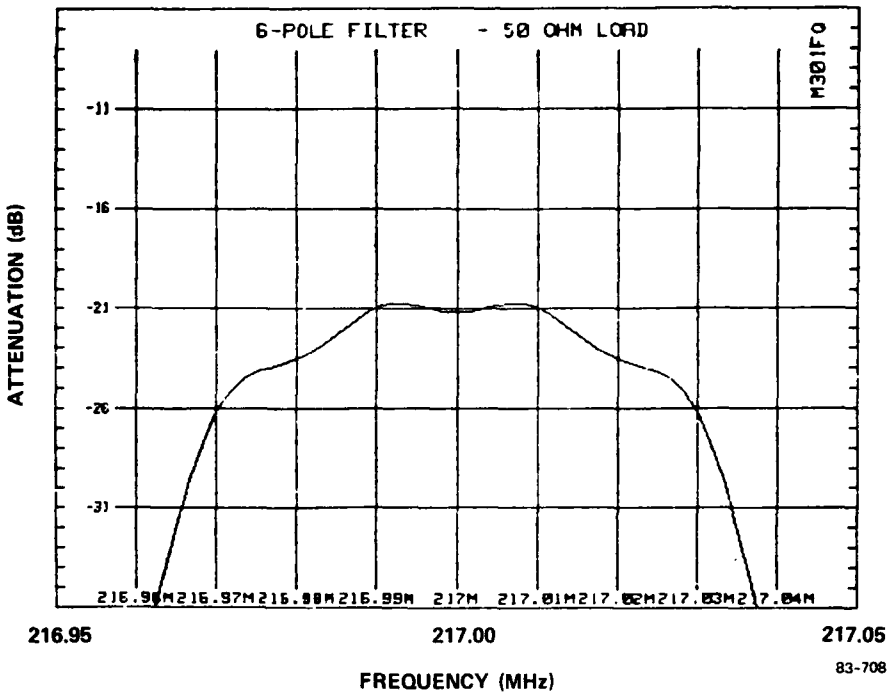

FIG. 29 Theoretical passband response of the six-pole filter loaded at the input and the output by 50 ohms without any matching. (Add 6 dB.)

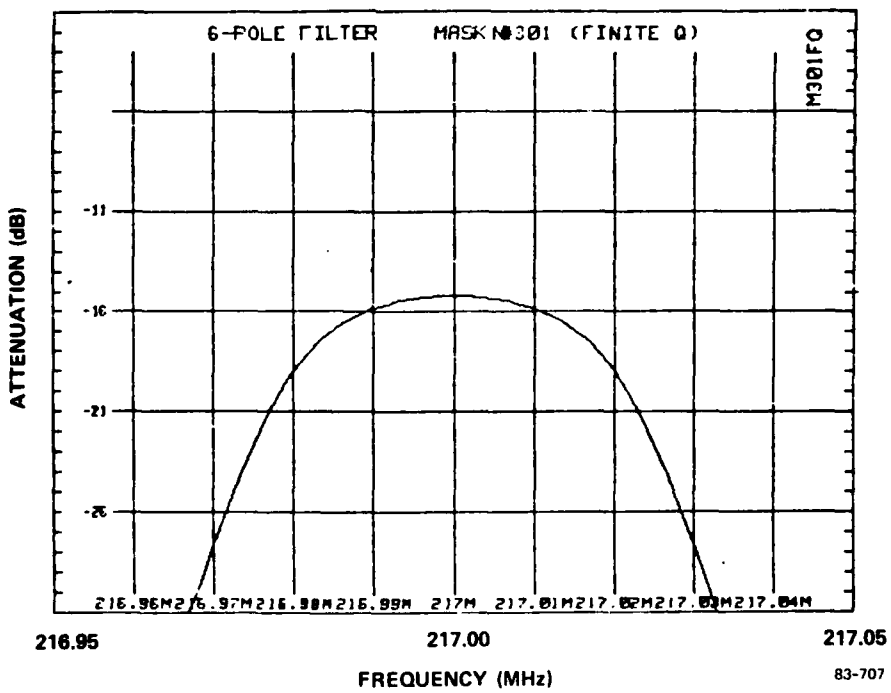

FIG. 30 Theoretical passband transmission characteristics of the six-pole (matched into 50 ohms) with resonator Q ≅ 18,000 (in atmosphere). (Add 6 dB.)

83-732

FIG. 31 Measured amplitude and return loss for unmatched six-pole filter.

environment (e.g., open- or short-circuit conditions) is simulated in the circuit analysis. The two important characteristics are the passband transmission response and the input/output reflection coefficient (s_{11}) with the other port open-circuited. These two response curves corresponding to the middle section and the input/output section of the filter are shown in Figures 32 through 36. This filter is designed to have a center frequency of exactly 217 MHz and is used as a reference. In practice, an actual filter at a slightly difference frequency can be compared to the reference filter by adjusting the frequencies of all the sections by the proper amount (i.e., 217 MHz - center frequency of the actual filter).

Figure 32 shows the transmission response, and Figure 33 shows the input return loss in dB (return loss = 20 log s_{11}) for the middle section. The output return loss is exactly the same as the input in this case because the middle section is symmetrically tuned. Figure 34 is the transmission response of the input/output section. This section is not tuned symmetrically; i.e., the resonance frequency of the first cavity is different from the frequency of the second cavity. Thus the return loss for the first cavity is shown in Figure 35, and that for the second cavity is shown in Figure 36. The first cavity corresponds to the input and the output ports of the whole filter (Poles 1 and 6) and the second cavity corresponds to Poles 2 and 5.

The coupling strength can be determined by observing the transmission response of the devices. If other parameters are kept constant, the coupling is directly proportional to the 3 dB bandwidth. The measured bandwidth is compared with the circuit analysis results for the corresponding section and, if necessary, adjusted by trimming the coupling array.

INPUT=NODE 1	OUTPUT=NODE 8		GROUND=NODE 0	
COMPONENT	VALUE	PERCENT TOLERANCE	NODE CONNECTIONS FROM,	TO,(+),(-)
RESISTOR 1	50 ohm	0	1	2
RESISTOR 2	50 ohm	0	8	0
RESISTOR 3	30 ohm	0	3	4
RESISTOR 4	30 ohm	0	6	7
CAPACITOR 1	3.38 pF	0	2	0
CAPACITOR 2	3.38 pF	0	8	0
CAPACITOR 3	13.3 pF	0	5	0
CAPACITOR 4	1.46 fF	0	4	5
CAPACITOR 5	1.46 fF	0	7	8
INDUCTOR 1	368.534674491 uHy	0	2	3
INDUCTOR 2	368.534674491 uHy	0	5	6

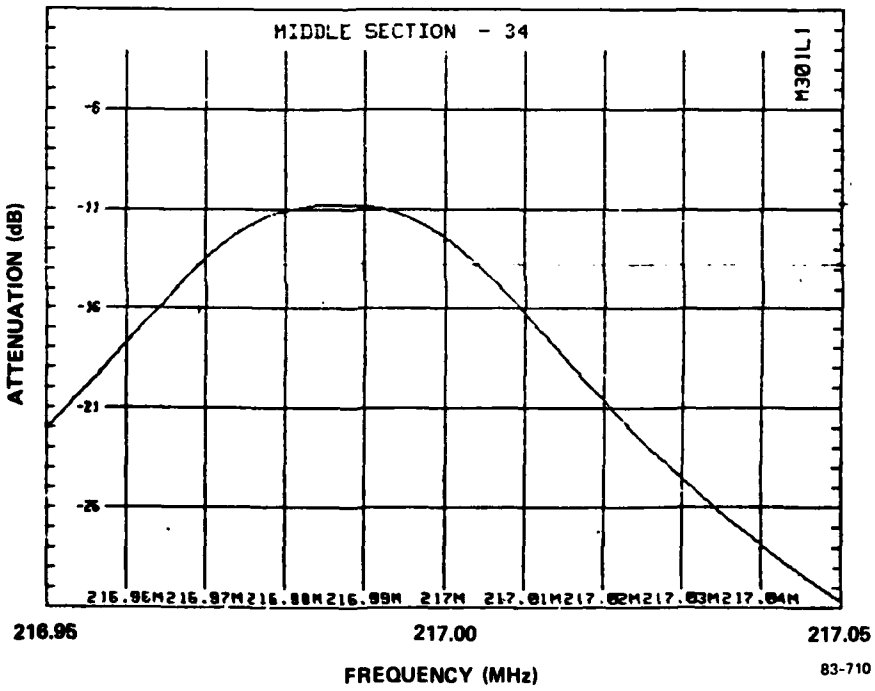

FIG. 32 Passband transmission response for middle section of filter. (Add 6 dB.)

IMPEDANCE NODE = 8

COMPONENT	VALUE	PERCENT TOLERANCE	NODE CONNECTIONS FROM,	TO,(+),(-)
RESISTOR 1	50 ohm	0	1	2
RESISTOR 2	10 Gohm	0	8	0
RESISTOR 3	32 ohm	0	3	4
RESISTOR 4	32 ohm	0	6	7
CAPACITOR 1	3.38 pF	0	2	0
CAPACITOR 2	3.38 pF	0	8	0
CAPACITOR 3	13.3 pF	0	5	0
CAPACITOR 4	1.46 fF	0	4	5
CAPACITOR 5	1.46 fF	0	7	8
INDUCTOR 1	368.534674491 uHy	0	2	3
INDUCTOR 2	368.534674491 uHy	0	5	6

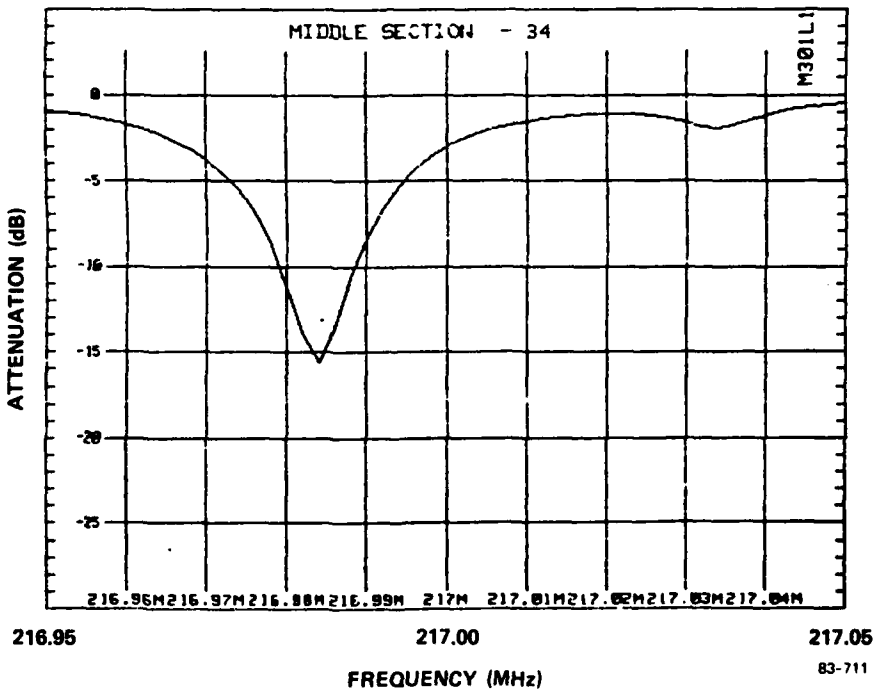

FIG. 33 Input return loss (20 log s_{11}) for middle section of filter.

INPUT=NODE 1 OUTPUT=NODE 8 GROUND=NODE 0

COMPONENT	VALUE	PERCENT TOLERANCE	NODE CONNECTIONS FROM,	TO,(+),(-)
RESISTOR 1	50 ohm	0	1	2
RESISTOR 2	50 ohm	0	8	0
RESISTOR 3	34 ohm	0	3	4
RESISTOR 4	34 ohm	0	6	7
CAPACITOR 1	2.83 pF	0	2	0
CAPACITOR 2	2.83 pF	0	8	0
CAPACITOR 3	4.64 pF	0	5	0
CAPACITOR 4	1.15 fF	0	4	5
CAPACITOR 5	1.15 fF	0	7	8
INDUCTOR 1	467.875780346 uHy	0	2	3
INDUCTOR 2	467.929046019 uHy	0	5	6

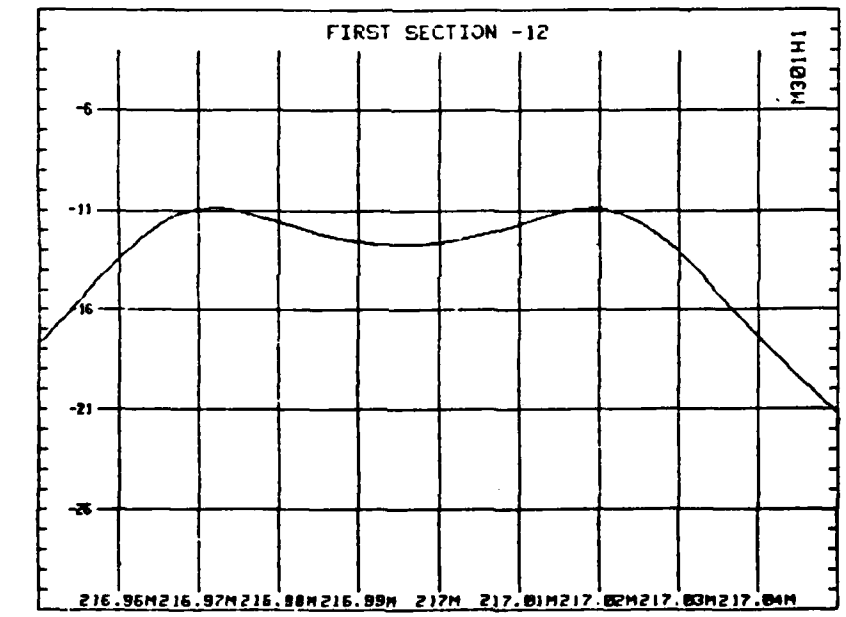

216.95 217.00 217.05

FREQUENCY (MHz)

83-712

FIG. 34 Passband transmission response for input/output section of filter. (Add 6 dB.)

IMPEDANCE NODE = 8

COMPONENT	VALUE	PERCENT TOLERANCE	NODE CONNECTIONS FROM,	TO,(+),(-)
RESISTOR 1	50 ohm	0	1	2
RESISTOR 2	10 Gohm	0	8	0
RESISTOR 3	34 ohm	0	3	4
RESISTOR 4	34 ohm	0	6	7
CAPACITOR 1	2.83 pF	0	2	0
CAPACITOR 2	2.83 pF	0	8	0
CAPACITOR 3	4.64 pF	0	5	0
CAPACITOR 4	1.15 fF	0	4	5
CAPACITOR 5	1.15 fF	0	7	8
INDUCTOR 1	467.875780346 uHy	0	2	3
INDUCTOR 2	467.929046019 uHy	0	5	6

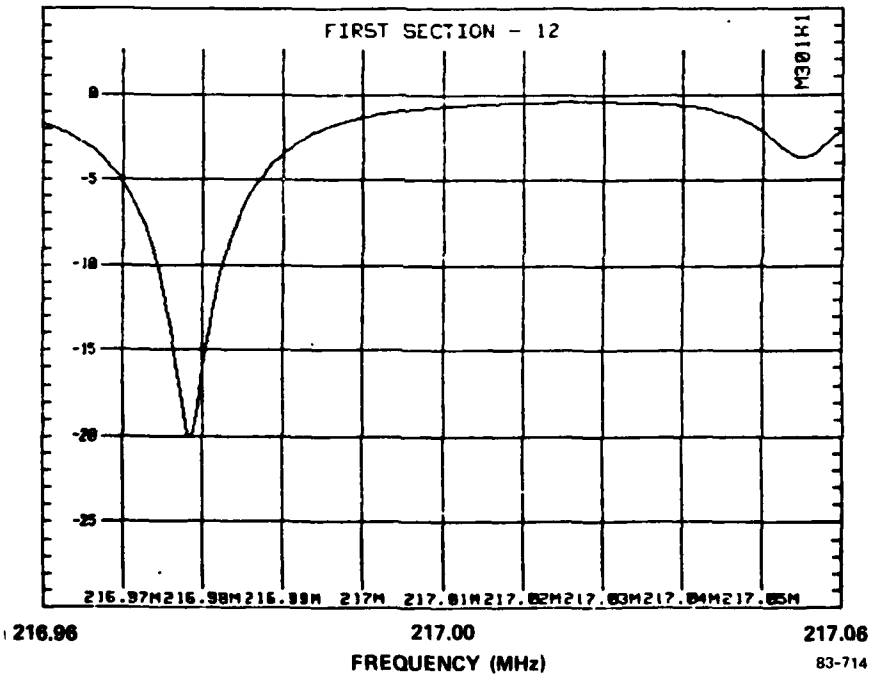

FIG. 35 Input return loss (20 log s_{11}) for first cavity of input/output section.

IMPEDANCE NODE = 8

COMPONENT	VALUE	PERCENT TOLERANCE	NODE CONNECTIONS FROM,	TO,(+),(-)
RESISTOR 1	50 ohm	0	1	2
RESISTOR 2	10 Gohm	0	8	0
RESISTOR 3	34 ohm	0	3	4
RESISTOR 4	34 ohm	0	6	7
CAPACITOR 1	2.83 pF	0	2	0
CAPACITOR 2	2.83 pF	0	8	0
CAPACITOR 3	4.64 pF	0	5	0
CAPACITOR 4	1.15 fF	0	4	5
CAPACITOR 5	1.15 fF	0	7	8
INDUCTOR 1	467.875780346 uHy	0	5	6
INDUCTOR 2	467.929046019 uHy	0	2	3

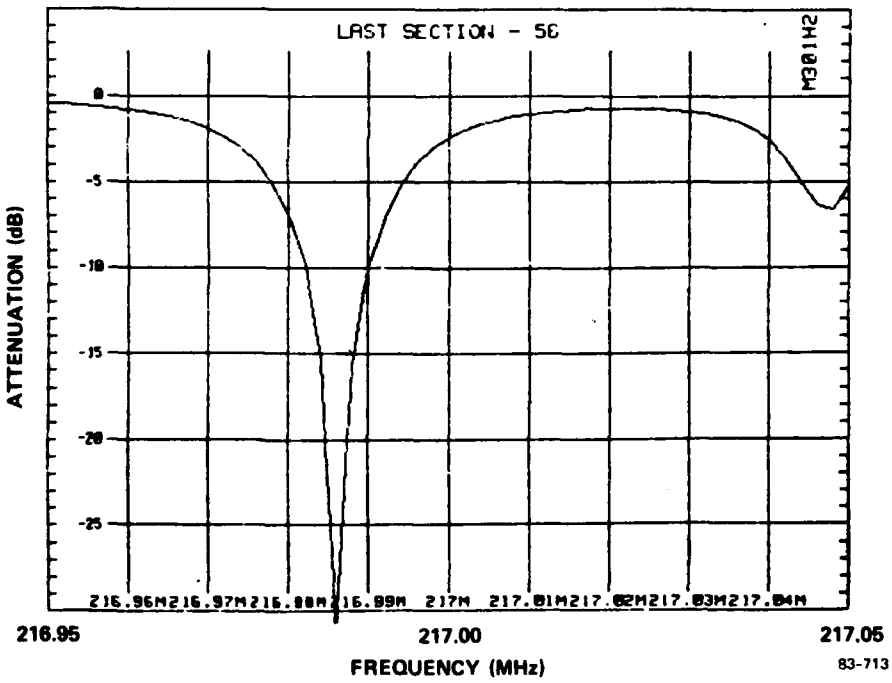

FIG. 36 Input return loss (20 log s_{11}) for second cavity of input/output section.

The input (or the output) reflection coefficient of the two-pole section usually displays two minima corresponding to the frequencies where the impedance is closest to 50 ohms (see Figure 36). The frequency at which the first minimum occurs, while not equal to the series arm resonance frequency (f_i) of the input pole, is compared directly with the corresponding theoretical first minimum to tune the input cavity to the desired frequency. The output cavity is similarly tuned. (The first minimum of the input reflection coefficient occurs at the resonance frequency of the entire circuit including the static capacitances (C_{01} and C_{02}.) After all the cavities are tuned to the correct frequencies, the external capacitors C_{e1} and C_{e2} are added, and the three sections are connected together. The unmatched filter response is checked and compared with the predicted response (Figures 29 and 31). Then the filter is matched in its holder for the best response, and the construction is completed.

SECTION 4

DEVICE FABRICATION

4.1 PHOTOLITHOGRAPHY

We now describe the device fabrication process including substrate selection, design of the photomask, processing, trimming, and packaging.

We have chosen to use two-inch diameter/.020" thick "ST" cut quartz discs as the substrate for each filter. Our goal was to fabricate all elements of the filter on a single substrate, but for improved yield we fabricated the filters in separate two-pole sections. The quartz discs were chosen for use because they are compatible with our mask aligner and we have more than adequate surface area for the complete device. Several suppliers have been used for this material and we have found that, first of all, discs of this size are very expensive (on the order of a hundred dollar each) if they do not include a "seed" crystal down the center, and secondly crystals with growth defects such as twinned zones and areas with high dislocation densities are sometimes received. Since we cannot fabricate a device on the seed because in general they will not function properly, we must know where the seed is and then make provision for placing the resonators elsewhere. This we accomplish by having the vendor outline the seed position on the unpolished side of the substrate. We then offset the filter sections on the mask so as to avoid the seed which is usually in the crystal center consisting of a long narrow strip parallel to the X axis. Frequently the seed edge is very pronounced and can be seen when properly held to the light. To further ensure that the quartz is adequate, we specify that all substrates are to be cut from the same stone, and we chemically etch one substrate from each lot in a solution of buffered hydrofluoric acid for a day or so. Imperfections in the crystal are clearly highlighted by this procedure. We had one lot of quartz of particularly poor quality and resonator sections, though not

placed on the seed, were very often significantly different in frequency and Q value. In addition, thermal stresses, on imperfect quartz, which occur during rapid (20°C)/Min) heat cycle would often cause a resonant section to shift upward in frequency by about 4 percent on this poor material. This indicated that twinning had occurred due to the propagation of dislocation from an already twinned zone. The crystals are also made with a flat about one inch long, which may be parallel or normal to the X-axis, to properly align the resonators with the X direction of propagation.

The photolithographic mask is produced by writing optical-pattern-generator flash instructions on a magnetic type an sending this tape to one of several mask houses. Since the resonators are fairly "regular", as are most surface wave devices, we have prepared computer subroutines which may be called to produce the flash instructions for a two-pole acoustically coupled pair. The subroutines are called with a relatively few number of arguments necessary to specify the structure. New mask designs are therefore implemented very quickly. For this relatively low frequency work in the VHF region we use iron oxide masks which are semitransparent. During processing we can see the substrate through the mask which facilitates alignment and allows us to ensure good mask-substrate contact. For higher frequency devices we must use low-reflectively chrome masks.

The device fabrication can be understood by reference to Figure . We clean and bake the substrate, and coat the substrate with about 1 micron of AZ-1470 photoresist. As shown in Figure 37, the entire device pattern (transducers, reflectors, bonding pads, etc.) is

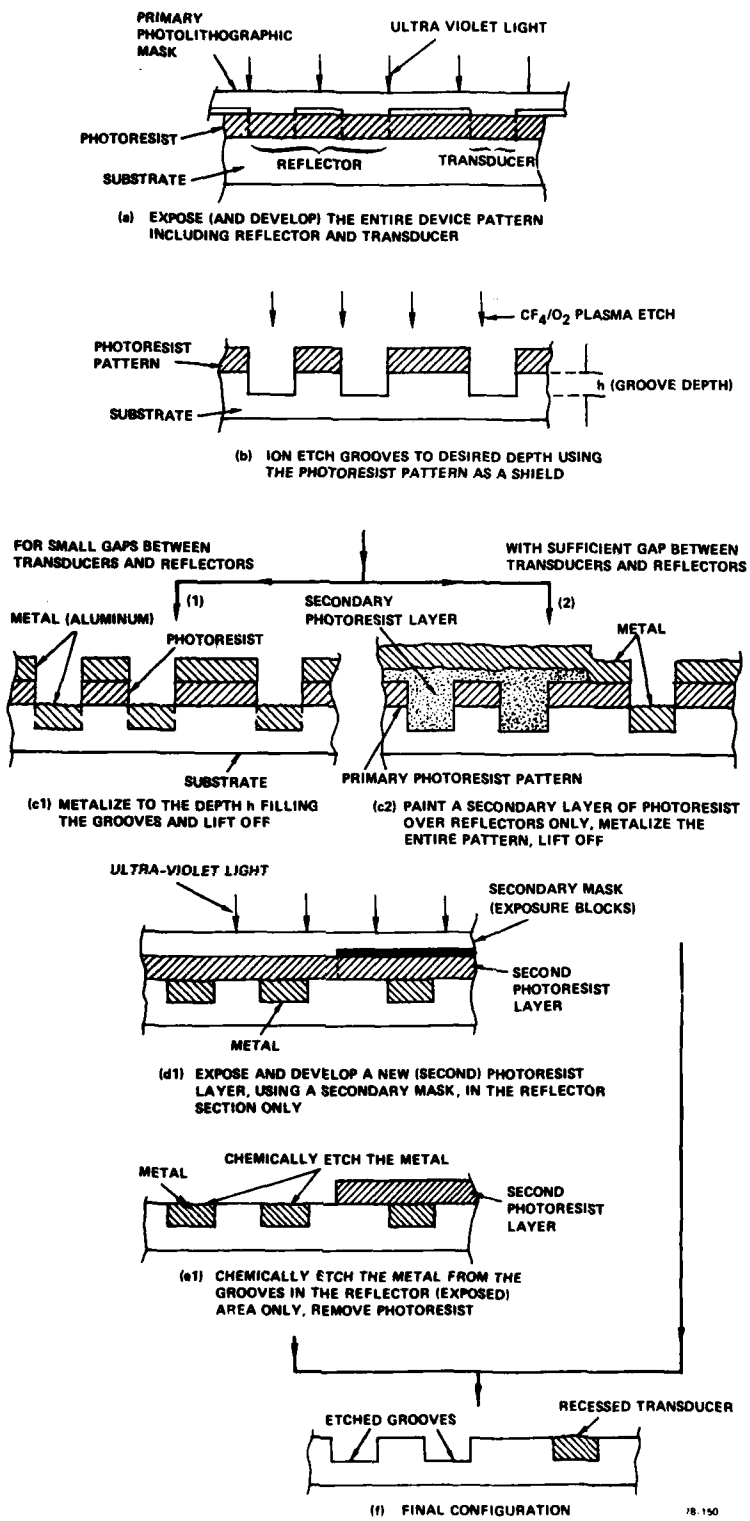

FIG. 37 Process steps required for fabrication of a recessed-transducer/grooved-reflector resonator system.

exposed and the photoresist pattern is developed. The entire pattern is then reactively etched, at low power (~ .1 watt/cm^2) to prevent photoresist bake-on, in a RF sputtering station with a CF_4 (80 percent) plus O_2 (20 percent) plasma. This gas mixture is used because we obtain highly reproducible etch rates (± 3 percent) without stringent operating procedures. This is so because etching is produced primarily by a chemical reaction between the ions in the plasma and the quartz. For the devices we etch to a depth of 2400 Å (.012 λ_0) and the Type I devices are etched to 1450 Å (.01 λ_0). After etching, the entire pattern is metalized with a bonding layer of chromium (100 Å) followed by aluminum (with about 3 percent copper to inhibit electro-acoustic migration of the electrode metal) thick enough to fill the grooves. This latter step is shown in Figure 37 (c_1). When enough space exists between the reflectors and transducers, we can follow step (c_2) and coat the reflectors with resist prior to metalizaton thus simplifying the procedure. However, for the devices in this program we kept the spaces small and therefore followed step (c_1) to improve our yield. Following metalization we then lift-off the unwanted metal, by immersing the substrate in acetone, yielding recessed transducers, and reflector grooves filled with metal (to be removed). After recoating the device with resist, we use the exposure blocks, seen on the mask of Figure 36 , to expose only the device reflectors and develop the resist away per Figure 39 . The metal in the reflectors may then be chemically etched away, using commercial aluminum and chrome etchants. For two-pole acoustically coupled cavities we only remove the aluminum. We leave the thin chrome layer at the base of the reflector grooves to act as a mask which allows us to selectively etch (in a CF_4 + O_2 plasma) the quartz (ridge tops) reducing the ridge height and the reflectivity of the structure. By this means, shown in Figure 38, we can increase the coupling between acoustically-coupled cavities after fabrication. Finally, we recoat the device with resist to protect the structures and dice the wafer.

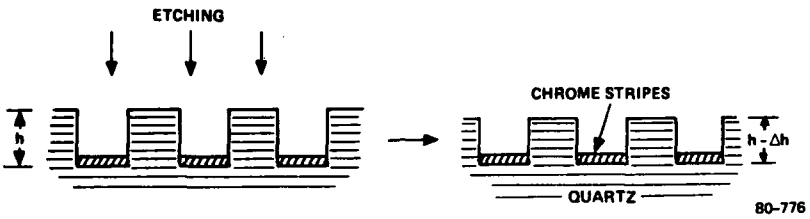

FIG. 38 Section view illustrating a technique for varying the coupling (by changing the groove depth) of grooved grating-couplers on quartz.

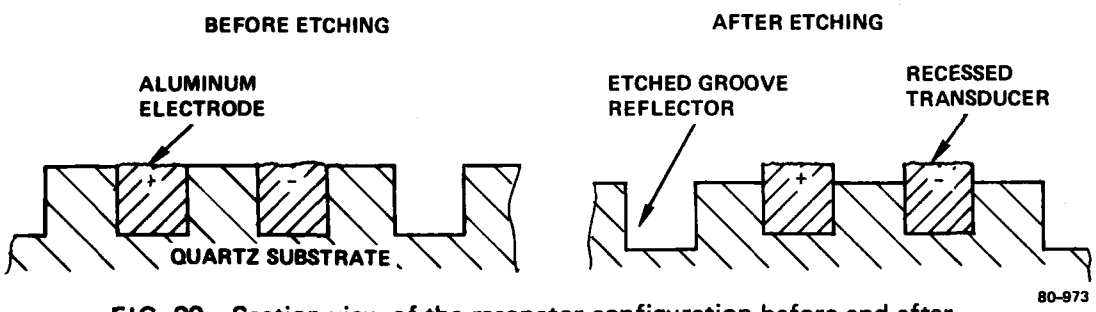

FIG. 39 Section view of the resonator configuration before and after selectively etching the quartz substrate in a tetrafluormethane (CF_4)-plus-oxygen plasma.

4.2 FREQUENCY TRIMMING

The device is cleaned by removing the resist in acetone and by exposing the entire device to the CF_4/O_2 plasma in the RF sputtering station for about one minute. We have found this to be a very effective cleaning procedure as evidenced by increased Q values following such exposure. The frequency of each resonator cavity is then found by using a set of microprobes. Each cavity remains isolated and no leads are bonded on until all cavities and reflectors are trimmed to specification. The resonant frequencies and two-pole pair responses are all measured, as discussed in Section 3, and recorded. The frequency of each cavity is then trimmed downward to the required value, and the reflector-coupling values adjusted as necessary.

To frequency trim each cavity, we selectively etch the quartz in a CF_4/O_2 plasma by RF sputtering. The change in device configuration is shown in Figure 39 . In this process the aluminum electrodes remain substantially unchanged (etch rate difference on the order of 10:1 are generally obtained) while the quartz is removed in a uniform manner. When performing this trim procedure, we shield all portions of the structure, using ungrounded metal masks, which we do not wish to expose to the plasma.

The etching process may be perfomed by RF sputtering or plasma-assisted etching, processes which are discussed Ref. 23, Sections II-1 and V-2, respectively. The gas mixture we use is CF_4 (80 percent) + O_2 (20 percent) by volume, though the percentage of O_2 is not critical, and our trimming is usually performed in an RF sputtering station with a backfill pressure of about 20μ (of Hg) at a power density in the range of 0.1 W/cm^2. We have successfully performed device trimming in a very simple barrel-type plasma reactor though the trim rates are much lower than for RF sputtering. The etching of the quartz is performed by chemically reactive ions formed by disassociation of the CF_4. The function of the O_2 is to suppress fluorocarbon-polymer

formation (which coats the device surface in the absence of O_2) and to enhance etching by the formation of an oxyfluoride (OF) species and by increasing the fluorine-carbon ratio. The frequency trim rate for a given device design is established empirically by subjecting a device to the etching process for a given length of time. We generally trim a device to frequency using an iterative procedure so as not to reduce the frequency below that which is desired. Also, the devices are designed and fabricated to have an initial frequency higher than the final frequency desired. The maximum trimming range for resonators being made is approximately 500 parts-per-million. An experiment was performed using a section of the 217 MHz resonator where the transducer was deeply recessed, Figure 40a. The substrate was then etched in several steps to the final geometry, Figure 40b and the frequency measured at each step. The results are plotted in Figure 41 and indicate the maximum frequency, and therefore velocity, is where h = ~1000 Å indicates that in production this configuration would be the least sensitive to processing variations. The quantitative results in Figure 41 are device dependent since the transducer section forms only a portion of the cavity; however, the qualitative results are general and would apply to all resonators. This range is adequate to compensate for the maximum device-to-device frequency variations of several hundred ppm we experience for our devices. Our photomask designs and fabrication procedures allow consistent attainment of an initial device frequency close enough to the desired frequency such that this trimming procedure may be successfully applied. We can trim our cavity resonance frequencies to an accuracy of 5 ppm which calculations show is acceptable for the filters under consideration here. The dominant effect of increasing the transducer step height for resonators is to increase the surface-wave reflectivity of the electrodes. A downward shift in the cavity resonance frequency occurs due to the stronger interaction between the waves reflected from the transducers and those reflected by the reflectors as the transducer reflectivity is increased. There is also a downward shift of the surface wave velocity under the transducer, however, calculations show that this has a minor effect on

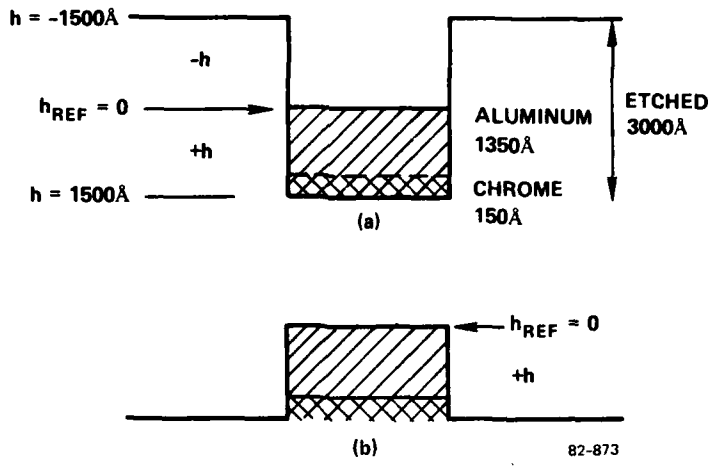

FIG. 40 Deeply recessed transducer (a) before RIE trimming and (b) after RIE trimming.

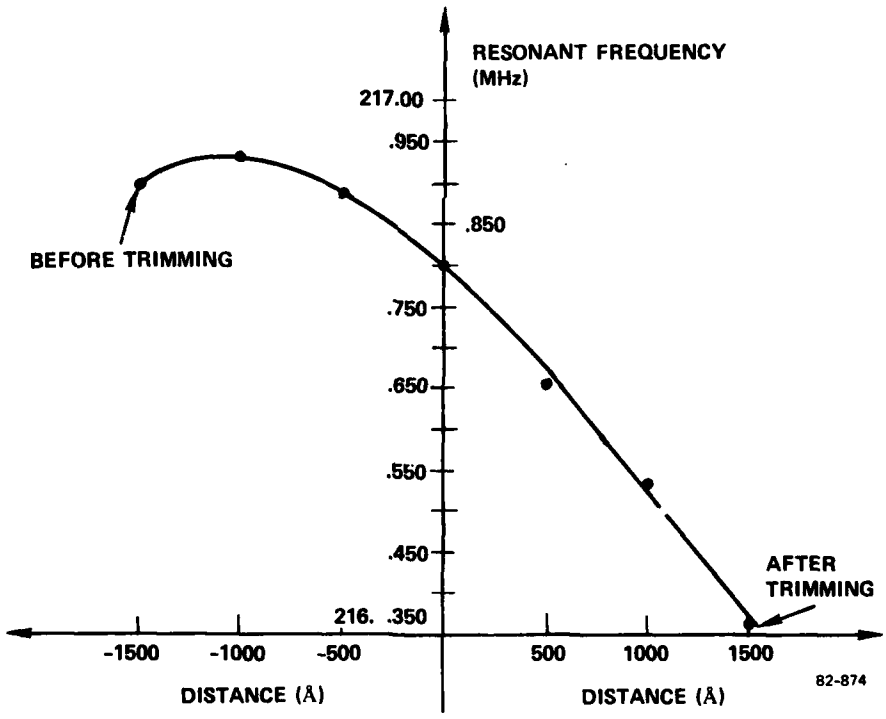

FIG. 41 Resonant frequency vs. substrate distance (h) from top of metal film for a single pole, two-pole test resonator.

resonator cavity frequencies. This trimming process is discussed in more detail in Ref. 17. For the devices in this program, we have found the trim rates to be in the range of 0.2 kHz/sec of etch which is slow enough to allow for very good control.

In trimming the reflector to adjust inter-cavity coupling we initially etched only the coupling reflector and shielded the outer reflectors (which also had the chrome removed). We found, however, that the rejection of these two-pole structures degraded significantly. By modeling the devices on the computer we were able to duplicate the experimental results and by calculation we found that etching all three reflectors eliminated this degradation. What happens when only the center reflector is etched is that the symmetry of the each cavity is broken in large measure due to the change in the phase, Φ, of the reflection coefficient for the center reflector. For long transducers we rely on a symmetric system to suppress the M±1 (where M is the mode number for the resonance) longitudinal modes, and these modes increase in level degrading the rejection when the symmetry is destroyed. Thus we leave the chrome in all three reflectors and etch all three together, while shielding the transducers, as needed to attain the necessary coupling.

4.2 PACKAGING OF PHASE I DEVICES

After the device has been fabricated and all cavities and reflectors trimmed to specification, the leads (one mil aluminum wire) are bonded to connect all structures as desired. Also to add flexibility, we placed the input/output matching L and C's on a circuit board external to the package and experimented with inductors in place of the coupling capacitors. We also split two devices into three separate sections, mounted them in separate headers, and placed the headers in circuit boards which allowed adjustment of the coupling components. We note here that once a device is fabricated with matching/coupling components on the substrate and leads bonded on, it is almost impossible to make a change without degrading the

performance of the device. This is so because bonding leads often becomes impossible, and working with adhesive or silver paint (for lead bonding) inevitably contaminates these very sensitive devices irreversibly. For each device response to be discussed in the experimental section we shall indicate how the device was configured.

The completed substrates were then bonded to the heavy lead-pins of the Type D[21] (1.3" diameter) header shown in Figure 42 using a gold filled epoxy[22]. The aluminum leads were then epoxied to the appropriate header pins, and a lid was cold-welded to the header in a high vacuum (~ 10^{-7} torr). The first serious problem we ran into in this procedure was that the substrates were subjected to varying levels of stress due to the fact of being rigidly bonded to a header with the lid sealed on. These stresses manifested themselves as a degredation, or complete disappearance, of the filter response. We found that the filter response could be made to vary by thermal changes or by mechanically stressing the sealed header. The only cure we had for this was to "nibble"[23] the lip of the header off thereby removing the lid and relieving the stresses. It turns out that the header and the lid may not both be perfectly planar where they join. The lid, being more rigid due to its structure, forces the header to conform to he shape of the lid lip when the seal is made in the press. On some devices the resulting header distortion so stressed the substrate that the device failed to work. We did not find these things out until we were sealing our devices for delivery at the end of phase I since we were just able to bring everything together (cold-weld-sealing, device fabrication, etc.) in the final month. We lost several devices right at the end due to irreversible damage before we discovered the nature of the problem. In addition, several of the devices delivered had their lids removed to relieve the stresses, and then the lids were replaced by soldering in several spots to act as a dust cover.

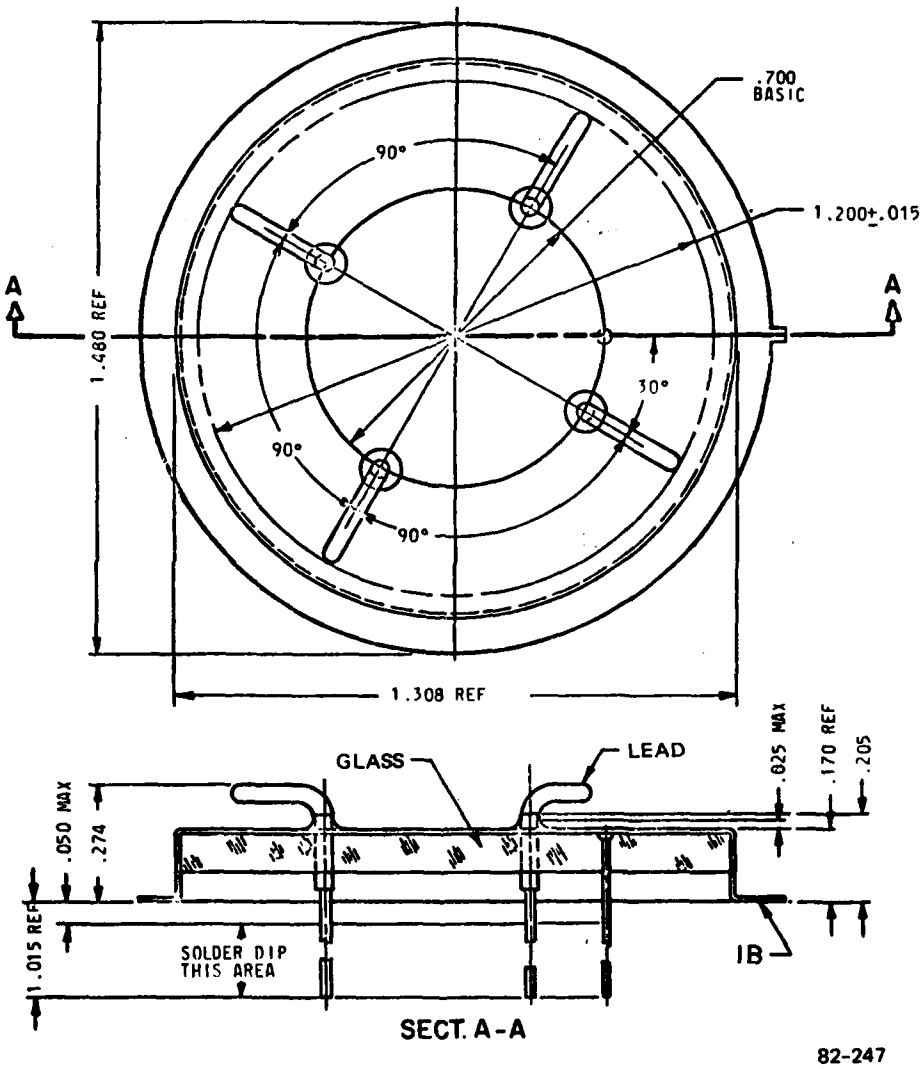

FIG. 42 Diagram of the cold-weld-sealable Type D leader.

4.3 PACKAGING OF PHASE II DEVICES

The packaging problems, detailed in the previous section, of the Phase I devices indicate a re-examination of the approach taken. While the cold welding of the Type D header, Figure 42 , offers cleaniness and the potential for good long term aging, there are serious mechanical stresses in the package when it is sealed under vacuum that degrade the device performance. Rather than tackle the mechanical engineering problems of stress free vacuum sealing, a simpler approach using conventional flat packages and a helium backfill was adopted and proved satisfactory. Figure 43 shows the three sections of a Type I filter mounted in a Isotronics IP 1600A package. The geometry is such that all sections are mounted before trimming and can be accessed with RF probes during the trimming process. In addition, the multipole pin outs permit each section to be accessed and matched outside the package; a technique which was useful in characterizing new designs. The delivered devices used internal chip 4 pF coupling capacitors[24]. The helium backfill was used to reduce the "air" loading loss and reduces the loss on the Type I filter by 1 dB compared to a 1.7 dB reduction in vacuum. In both cases the 10 dB loss specification was met. The feedthrough level in this package was in the -90 dB region a big improvement over the Type D header. A small bell jar with RF leads that could be evacuated and backfilled with helium was used to test the filters under the various packaging schemes.

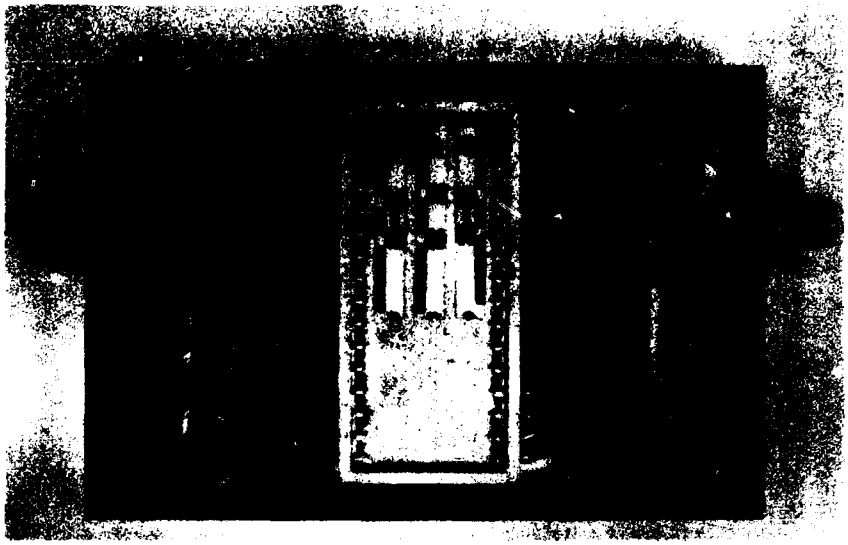

83-737

FIG. 43 Device No. 2 packaged in flatpack and brass block. Input and output matching components are outside the flatpack.

SECTION 5

EXPERIMENTAL RESULTS

The test results of the Type I and II filters for Phase I are in the Interim report, and since they did not meet the specification, will not be repeated here in this report.

5.1 TEST RESULTS OF THE DELIVERED TYPE I FILTERS

After sealing and backfilling with helium, the flat packages were mounted in machined brass packages and matched, Figure 43. The series inductor, an air-core coil, was about 70 nH and the shunt capacitor about 3 pF. These were adjusted slightly for each of the five filters. Table X shows the center frequency and the insertion loss for the five filters.

Table X

Filter	Center Frequency (MHz)	Loss (dB)
1	217.001	7.3
2	216.981	8.8
3	216.991	9.7
4	217.008	9.5
5	216.955	9.5

There was no attemp to make all the filters at the same frequency and with more care in the trimming the center frequencies can be made sufficiently close. The shape of the amplitude response, except for filter No. 5, has the

characteristic Butterworth response. Slight deviation from the ideal response can usually be accounted for by non-ideal frequencies of the individual poles. While the frequency of each pole is theoretically well known and can be trimmed as desired, it's control is the most troublesome aspect of the fabrication process--sometimes changing while the device is sitting overnight. Better process control associated with a larger volume of filters should reduce this problem.

The 2.3 dB variation in Q of the various sections and is a more serious problem, although the 10 dB loss specification was met. The Q's of the individual sections vary between 18,000 and 24,000 and are far from the theoretical limit of about 50,000. As mentioned in Section 2, there are several contributions to the overall device Q and it remains a problem in the technology to identify each contribution to the total Q.

The following figures record the wideband and narrowband amplitude, the narrowband reflection coefficient and impedance, and transfer phase of all five delivered devices.

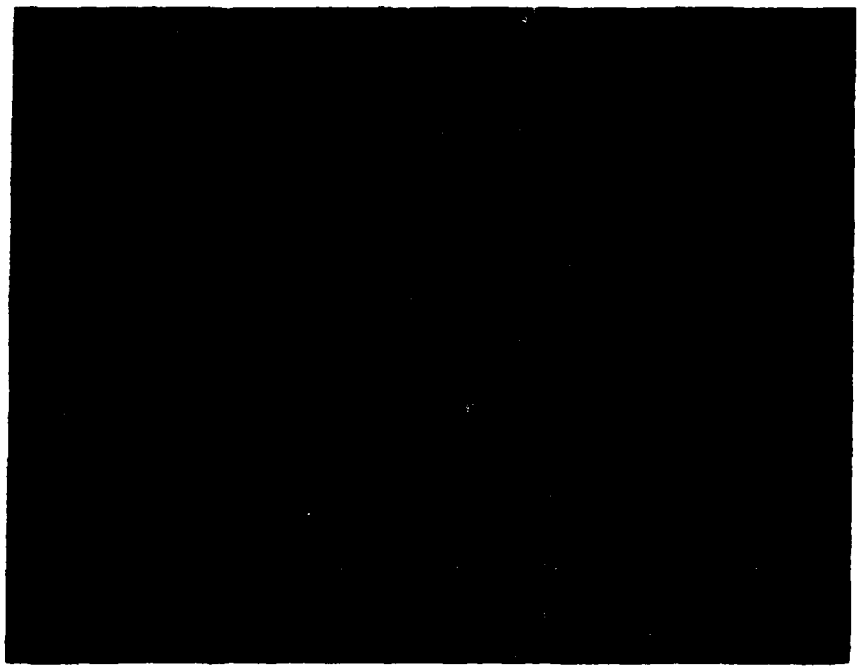

83-736

FIG. 44 Device 1 mounted in flatpack.

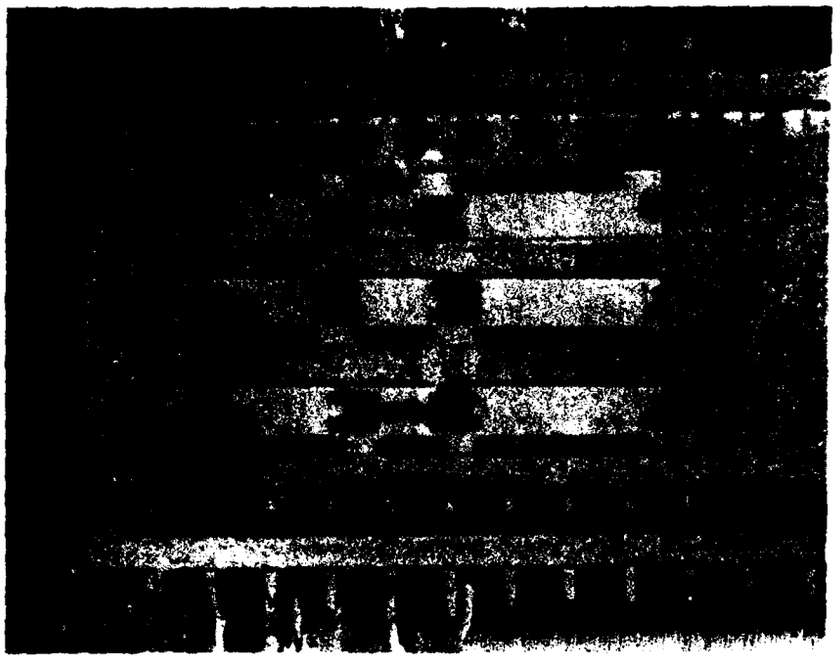

83-734

FIG. 45 *Device 2 mounted in flatpack.*

83-735

FIG. 46 Device 3 mounted in flatpack.

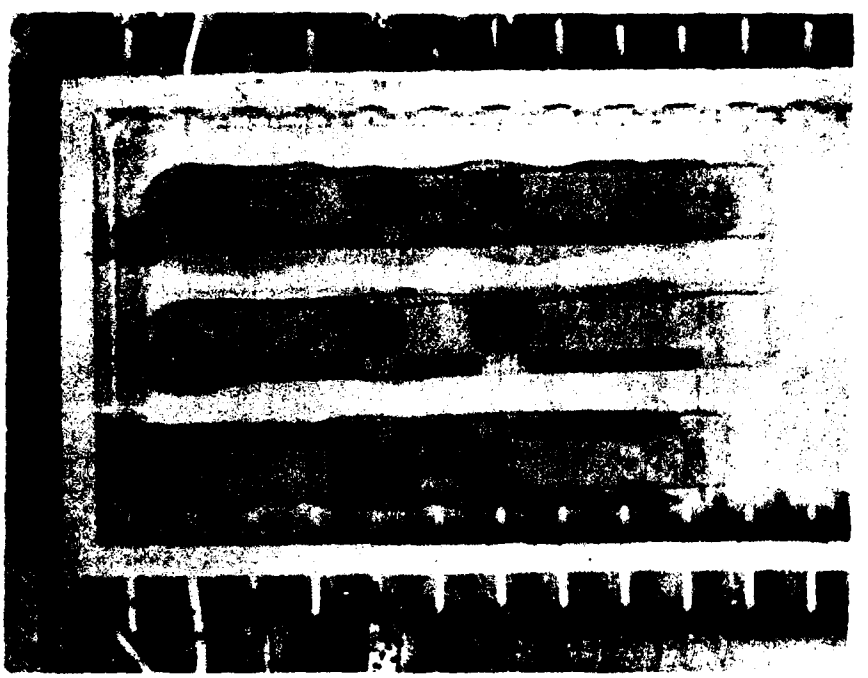

83-733

FIG. 47 Device 4 mounted in flatpack.

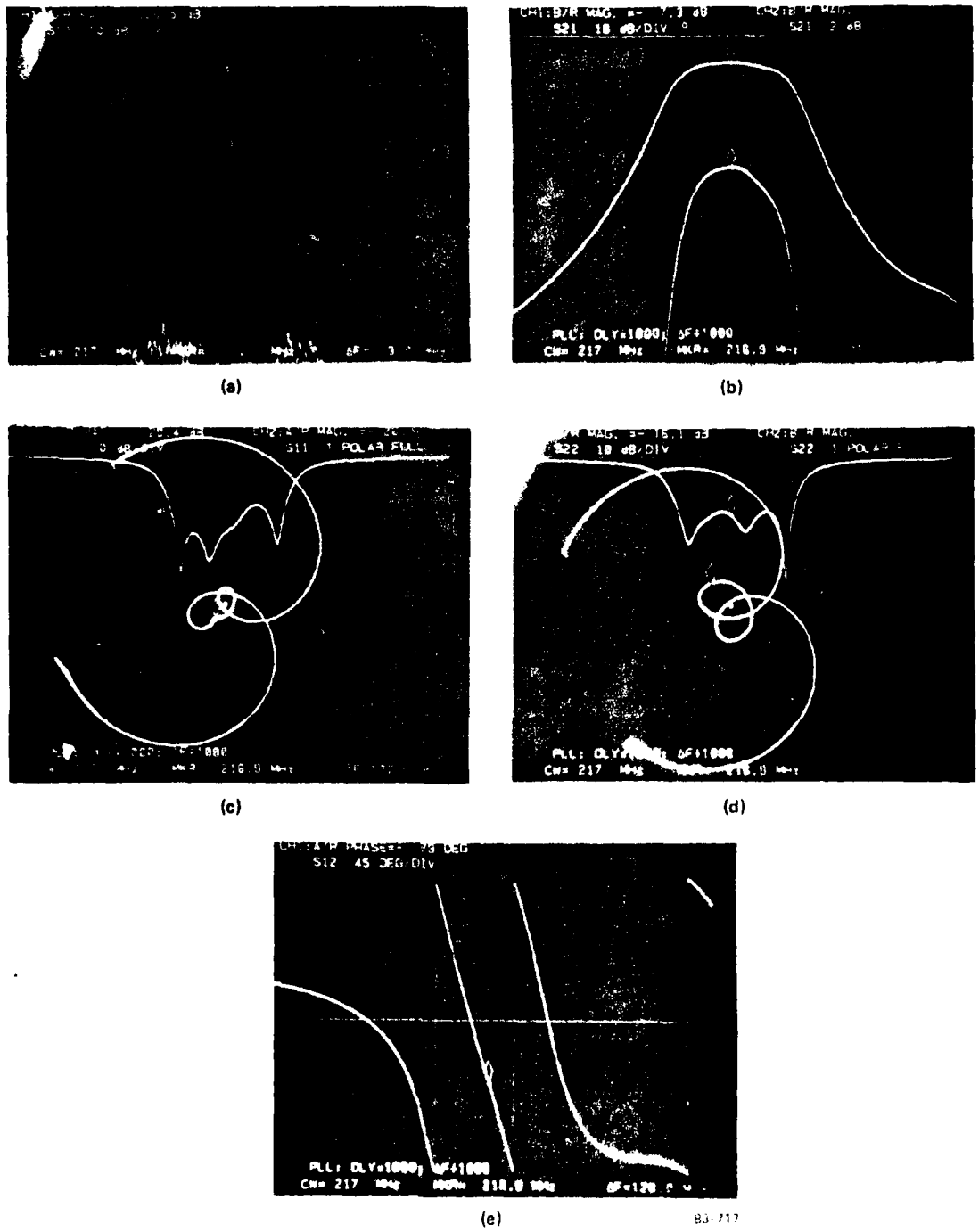

FIG. 48 Measured response of filter No. 1.

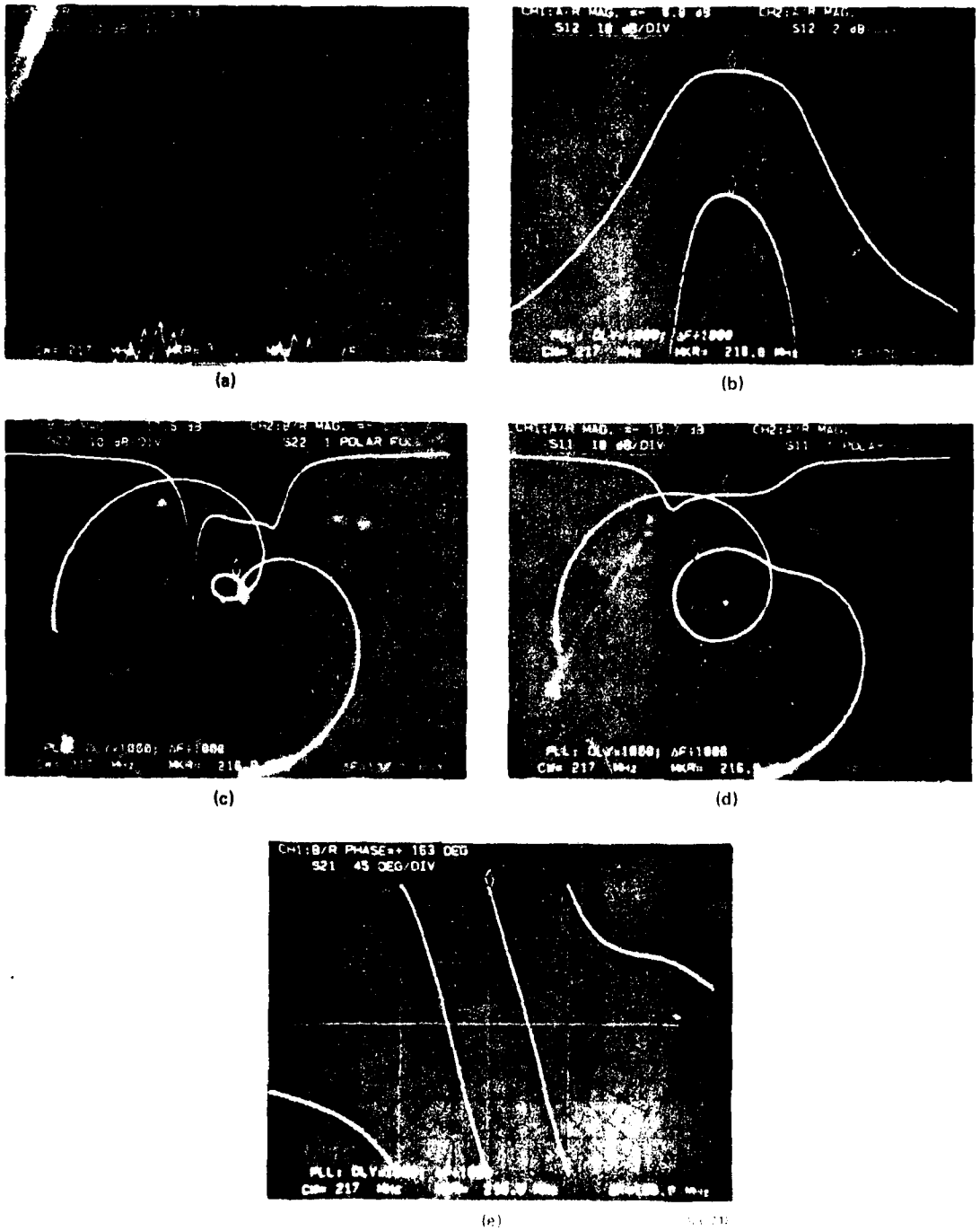

FIG. 49 Measured response of filter No. 2.

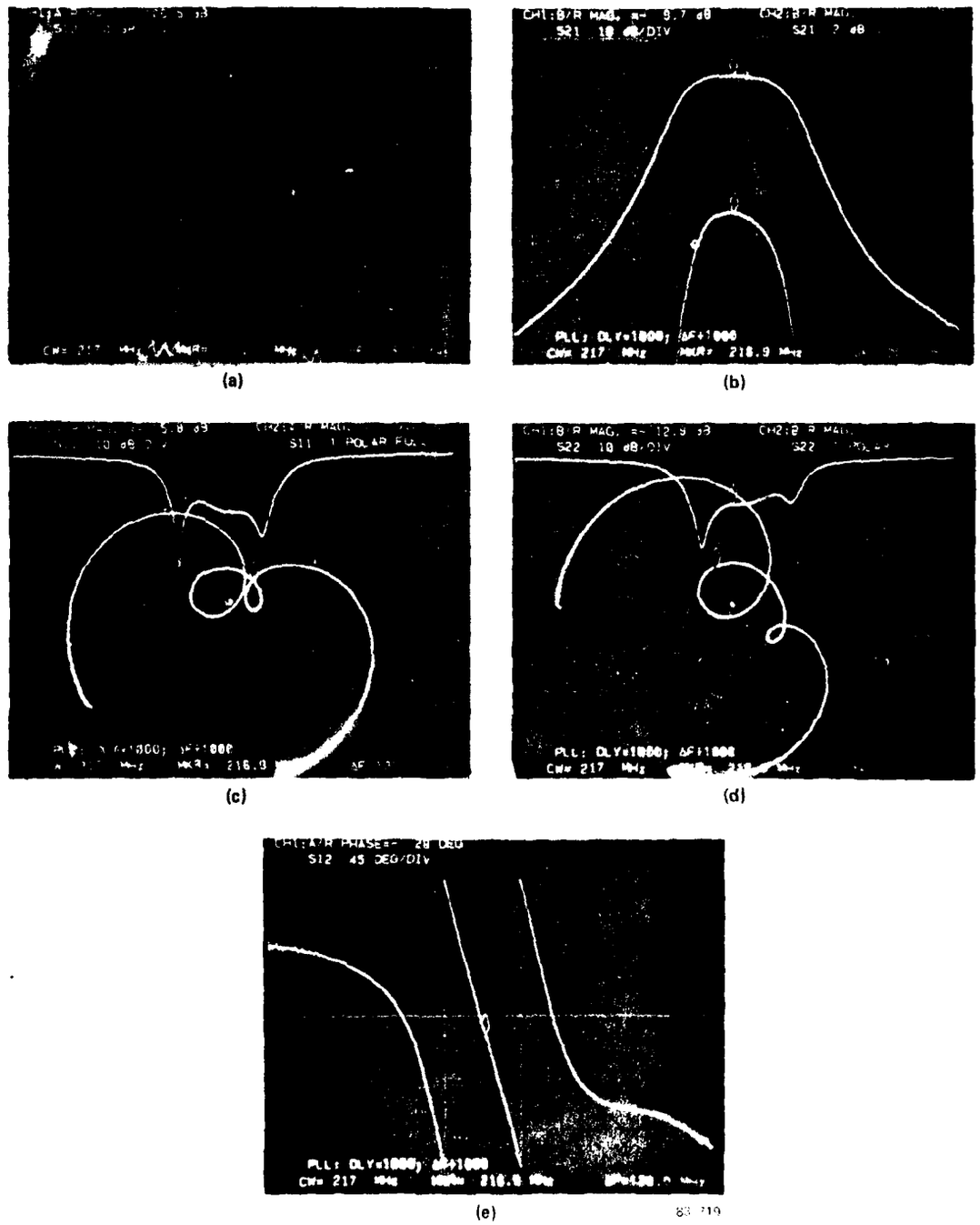

FIG. 50 Measured response of filter No. 3.

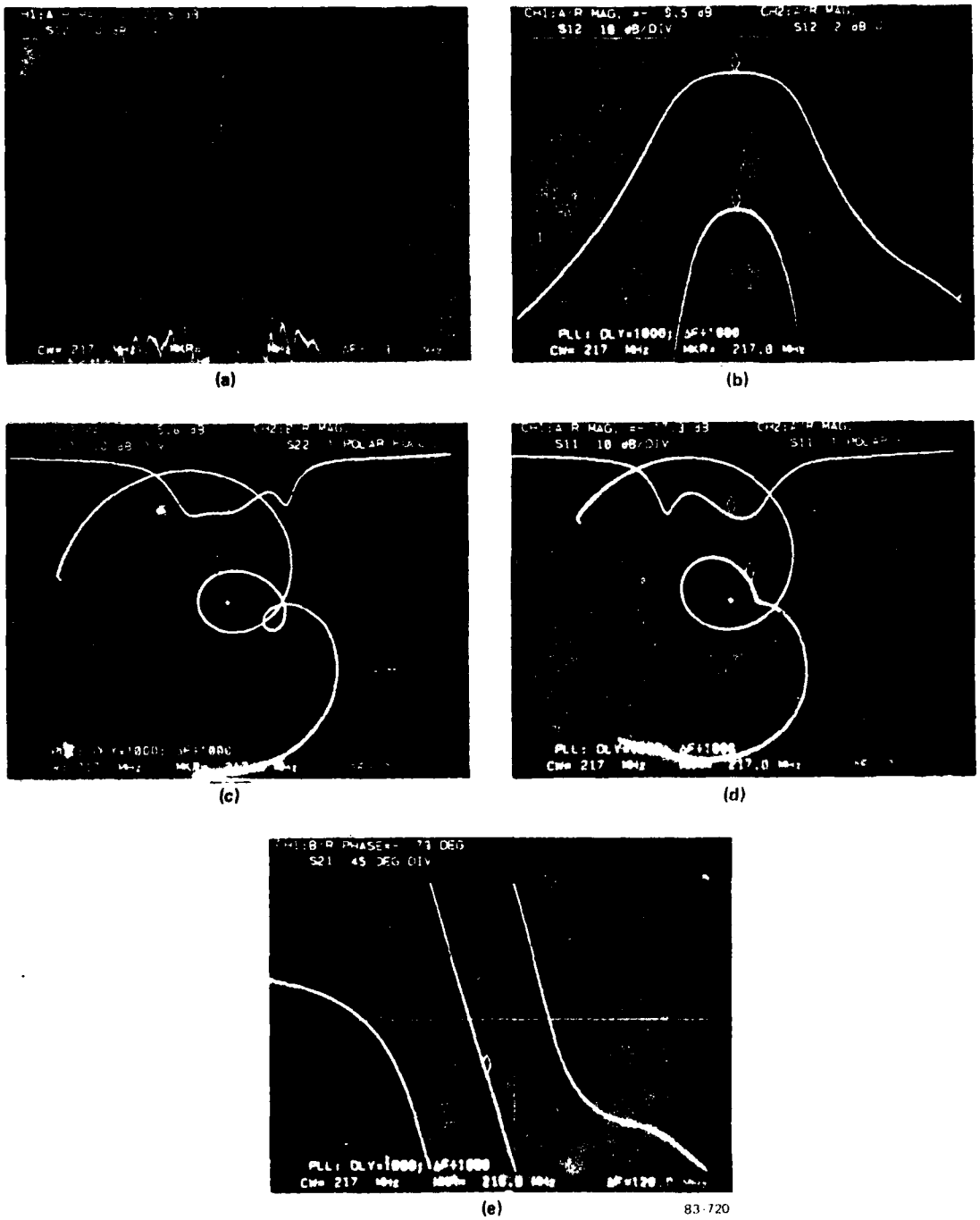

FIG. 51 Measured response of filter No. 4.

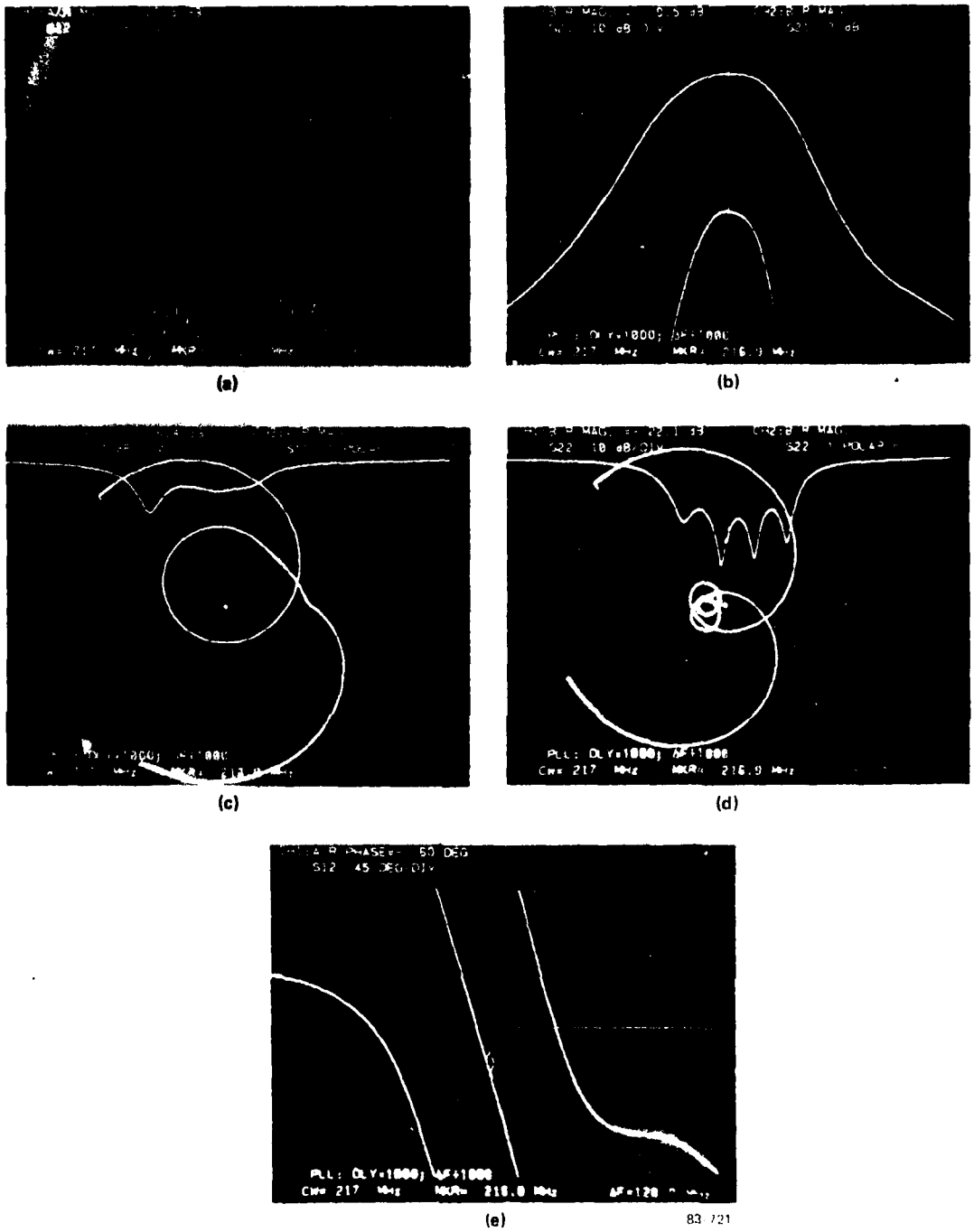

FIG. 52 Measured response of filter No. 5.

SECTION 6

CONCLUSION

The overall objectives of the contract, development of design and fabrication techniques for monolithic multipole filter were fulfilled. Five six-pole Butterworth filters with a center frequency of 217 MHz were designed, fabricated and delivered as required.

Based on our experience in this effort our assessment of multipole SAW Filter technology is that--

1. The existing synthesis procedures investigated, those of Matthaei or Rosenberg and Coldren, are sufficient to design the narrowband filters done here and there is no reason to suspect that wider bandwidth filters could not be designed.

2. There is room for improvement in SAW resonator analysis. Such areas as transverse mode control and the various loss mechanisms in the transducer and grating reflector are either not well understood or handled on an empirical bases. These shortcomings will be more noticeable at higher frequencies.

3. The combination of acoustic and transducer coupled sections works well for narrowband filters. The transducer coupling, which is necessary to reduce the out-of-band rejection, is not capable of strong coupling and would not be useful for wider bandwidth filters. If wideband filters are to be made, some form of strong coupling with good out-of-band rejection will have to be developed.

4. The building block approach and the L-C modeling of each section was indispensible to control the complex process of combining the six poles required for these filters. In addition to controlling the coupling between sections the frequency tolerance of each section is only a few parts per million, and it is relatively easy to degenerate into chaos.

5. In order for this technology to develop past the research stage there is a large amount of engineering to be done in the wafer processing and device packaging areas. There is no theoretical reason why SAW multipole filters could not be produced in volume at reasonable cost.

REFERENCES

1. A. I. Zvrev, "Handbook of Filter Synthesis," J. Wiley and Sons, New York (1967).

2. Matthaei, Young, Jones, "Microwave Filters, Impedance - Matching Networks, and Coupling Structures," McGraw-Hill, New York (1964).

3. "Reference Data for Radio Engineers," Fourth Edition, International Telephone and Telegraph Corp., New York, (1964).

4. H. J. Orchard, D. F. Sheahan, "Inductorless Bandpass Filters," IEEE Journal of Solid State Circuits, Vol. SC-5 No. 3, June 1970, pp. 108-118.

5. G. S. Matthaei, E. B. Savage and F. Barman, "Synthesis of SAW resonator filters using any of various coupling mechanisms," IEEE Trans. on Sonics and Ultrasonics, Vol. SU-26, pp. 72-84, March 1978.

6. R. L. Rosenberg and L. A. Coldren, "Scattering analysis and design of SAW resonator filters," IEEE Trans. on Sonics and Ultrasonics, Vol. SU-26, pp. 205-230, May 1979.

7. L. A. Coldren, R. C. Rosenberg and J. A. Rentschler, "Monolithic Transversely Coupled SAW Resonator Filters," Proc. of the 1977 Ultrasonics Symposium, pp. 888-893.

8. H. A. Simpson, E. D. Finch, Jr., R. K. Weeman, "Composite Filter Structures Incorporating Monolithic Crystal Filters and L C Network," Proc. 25th Annual Symposium on Frequency Control, 1971, pp. 287-296.

9. D. F. Sheahan, "Polylithic Crystal Filters," Proc. 29th Annual Symposium on Frequency Control, 1975, pp. 120-127.

10. W. J. Tanski, "High Q and GHz SAW Resonators," Proc. of the 1978 IEEE Ultrasonics Symposium, pp. 433-437.

11. W. J. Tanski and N. D. Wittels, "SEM observations of SAW resonator transverse modes," Appl. Phys. Lett., 34, No. 9, May 1979, pp. 537-539.

12. H. A. Haus, "Modes in SAW grating resonators," Jour. Appl. Phys. 48, No. 12, Dec. 1977, pp. 4955-4961.

13. W. J. Tanski, "Surface acoustic wave resonators on quartz," IEEE Trans. Sonics and Ultrasonics, Vol. SU-26, pp. 93-104, March 1979.

14. R. Chapman, E. G. S. Paige, M. W. Wagg, "The Deep Inlaid Interdigital Transducer," Proc. of the 1981 Ultrasonics Symposium, pp. 33-37.

REFERENCES (Cont'd)

15. M. B. Schulz and J. H. Matsinger, "Rayleigh-wave electromechanical coupling constants," Appl. Phys. Lett., Vol. 20, pp. 367-369, 1972.

16. M. B. Schulz, B. J. Matsinger, and M. G. Holland, "Temperature dependence of surface acoustic wave velocity on α quartz," J. Appl. Phys., Vol. 41, pp. 1-30, 1970.

17. W. J. Tanski, "SAW frequency trimming of resonant and travelling-wave devices on quartz," Appl. Phys. Lett., 39, No. 1, July 1981, pp. 40-42.

18. W. R. Smith, H. M. Gerard, J. H. Collins, T. M. Reeder, and H. J. Shaw, "Analysis of interdigital surface wave transducers by use of an equivalent circuit model," IEEE Trans. Microwave Theory Tech., Vol. MTT-17, pp. 856-864, Nov. 1969.

19. M. E. Field, R. C. Ho, and C. L. Chen, "Surface acoustic wave grating reflectors," Proc. 1975 Ultrasonics Symposium, pp. 430-433, (IEEE Cat. No. 75 CH9004-4SU).

20. R. C. M. Li and J. Melngailis, "The influence of stored energy at step discontinuities on the behavior of surface-wave gratings," IEEE Trans. on Sonics and Ultrasonics, Vol. SU22, pp. 189-198, May 1975.

21. W. R. Shreve, "Surface-Wave Two-Port Resonator Equivalent Circuit," 1975 IEEE Ultrasonics Symposium Proceedings, pp. 295-298.

22. DeVerl S. Humpherys, The Analysis, Design, and Synthesis of Electrical Filters, Prentice-Hall, Inc., 1970.

23. "Thin Film Processes" edited by J. L. Vossen and W. Kern (Academic Press, New York, 1978).

24. Semi-Films Division, National Microetics, Inc., CBA 10R-15RO-0004.

END

FILMED

1-84

DTIC